Monthly Notices of the ROYAL ASTRONOMICAL SOCIETY

MNRAS **467,** 3122–3139 (2017) doi:10.1093/mnras/stx125
Advance Access publication 2017 January 19

AE Ursae Majoris – a δ Scuti star in the Hertzsprung Gap

Jia-Shu Niu,[1,2,3] Jian-Ning Fu,[1⋆] Yan Li,[4] Xiao-Hu Yang,[1,5] Weikai Zong,[1,6,7] Hui-Fang Xue,[1] Yan-Ping Zhang,[1] Nian Liu,[1] Bing Du[5] and Fang Zuo[5]

[1]*Astronomy Department, Beijing Normal University, Beijing 100875, P.R. China*
[2]*CAS Key Laboratory of Theoretical Physics and Kavli Institute for Theoretical Physics China (KITPC), Institute of Theoretical Physics, Chinese Academy of Sciences, Beijing 100190, P.R. China*
[3]*School of Physical Sciences, University of Chinese Academy of Sciences, No. 19A Yuquan Road, Beijing 100049, P.R. China*
[4]*National Astronomical Observatories/Yunnan Observatory, Chinese Academy of Sciences, PO Box 110, Kunming 650011, P.R. China*
[5]*National Astronomical Observatories, Chinese Academy of Sciences, Beijing 100012, P.R. China*
[6]*Université de Toulouse, UPS-OMP, IRAP, Toulouse F-31400, France*
[7]*CNRS, IRAP, 14 avenue Edouard Belin, F-31400 Toulouse, France*

Accepted 2017 January 16. Received 2017 January 16; in original form 2016 April 5

ABSTRACT

We analyse the photometric data and spectroscopic data collected on the δ Scuti star AE Ursae Majoris (AE UMa). The fundamental and the first overtone frequencies are confirmed as $f_0 = 11.625\,60$ c d^{-1} and $f_1 = 15.031\,24$ c d^{-1}, respectively, from the frequency content by analysing light curves over 40 nights, spanning from 2009 to 2012. Additionally, another 37 frequencies are identified as either the harmonics or the linear combinations of the fundamental and the first overtone frequencies, among which 25 are newly detected. The rate of period change of the fundamental mode is determined as $(1/P_0)(\mathrm{d}P_0/\mathrm{d}t) = 5.4(\pm1.9) \times 10^{-9}$ yr^{-1} as revealed from the O − C diagram based on the 84 newly determined times of maximum light combined with those derived from the literature. The spectroscopic data suggest that AE UMa is a Population I δ Scuti star. With these physical properties, we perform theoretical explorations based on the stellar evolution codeMESA on this target, considering that the variation of pulsation period is caused by secular evolutionary effects. We finally constrain AE UMa with physical parameters as follows: mass of $1.805 \pm 0.055\,\mathrm{M}_\odot$, radius of $1.647 \pm 0.032 \times 10^{11}$ cm, luminosity of $1.381 \pm 0.048(\log L/\mathrm{L}_\odot)$ and age of $1.055 \pm 0.095 \times 10^9$ yr. AE UMa can be the (Population I) δ Scuti star that locates just after the second turn-off of its evolutionary track leaving the main sequence, a star in the phase of the Hertzsprung Gap with a helium core and a hydrogen-burning shell.

Key words: techniques: photometric – techniques: spectroscopic – stars: individual: AE UMa – stars: oscillations – stars: variables: δ Scuti.

1 INTRODUCTION

δ Scuti stars are a class of pulsating variable stars that lie in the classical instability strip crossing the main sequence (MS) on the Hertzsprung–Russell diagram. Their pulsations are driven by the κ-mechanism, which drives both the Cepheids and the RR Lyrae stars as well. The amplitudes of pulsations in δ Scuti stars are from mmag up to tenths of a magnitude, periods between 0.03 and 0.3 d (see, e.g. Niu, Fu & Zong 2013; Zong et al. 2015). These stars are found with masses between 1.5 and 2.5 $\mathrm{M}_\odot$, and luminosities between 10 and 50 $\mathrm{L}_\odot$. The general consensus shows that most (possibly all) δ Scuti stars are normal stars that evolve in the MS or the immediate post-MS stages, according to standard stellar-evolution theory (see, e.g. Baglin et al. 1973; Breger 1979, 1980). Nevertheless, an observational proof of the validity of this hypothesis has not been found yet (Petersen & Christensen-Dalsgaard 1996).

The high-amplitude δ Scuti stars (hereafter HADS) are traditionally found with slow rotation, with one or two dominant radial modes with amplitudes larger than 0.1 mag, although some of them may have low-amplitude non-radial modes (e.g. Poretti 2003). SX Phoenicis (SX Phe) stars is a subgroup of HADS with low metallicity and large spatial motion (see e.g. Fu et al. 2008b). They are old Population II stars and found to be members of globular clusters (Rodríguez & López-González 2000). However, some of them have been discovered in the general star fields (Rodríguez & Breger 2001). Interestingly, pulsations in the majority of the field SX Phe variables display simple frequency spectra with short periods

⋆ E-mail: jnfu@bnu.edu.cn

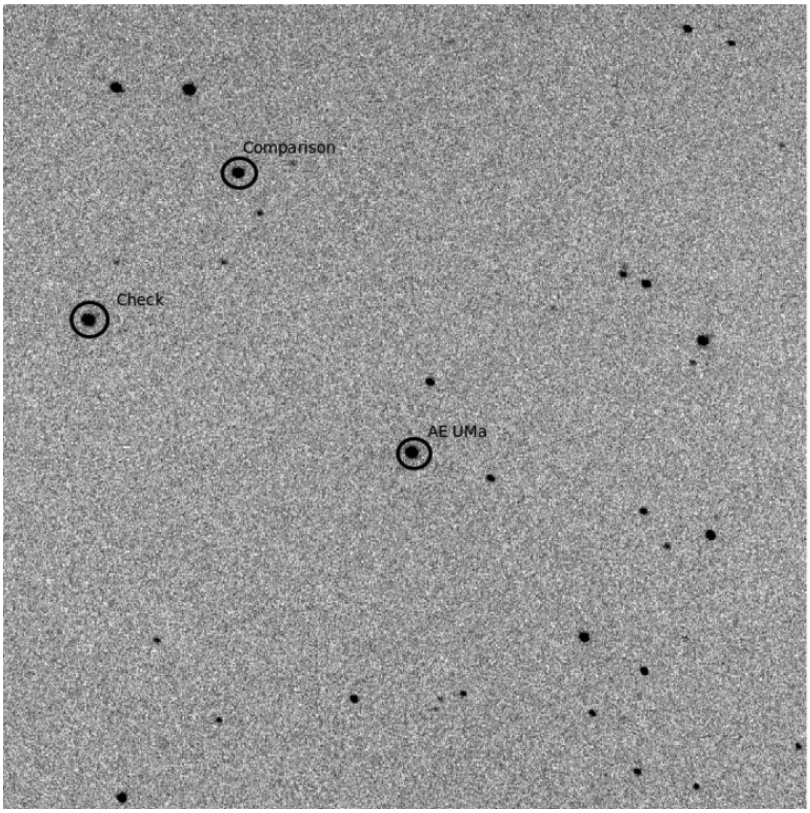

Figure 1. A CCD image (16.5×16.5 arcmin^2) of AE UMa ($\alpha_{2000} = 09^h36^m53^s$, $\delta_{2000} = +44°04'00''$) taken with the 85-cm telescope at the Xinglong station. North is down and east is to the right. AE UMa, the comparison star and the check star are marked.

Table 1. Journal of photometric observations in V for AE UMa with the 85-cm telescope.

CCD	Year	Month	Nights	Frames
PI BFT1024	2009	March	5	4055
	2009	May	3	516
	2010	February	2	1385
	2011	January	5	1275
	2011	February	8	4759
	2012	January	1	328
	2012	February	6	1887
PI BFT512	2012	March	5	2516
	2012	April	5	556

($\leq$0.08 d) and large visual peak-to-peak amplitudes ($\geq$0.1 mag; e.g. Fu et al. 2008a). The period changes of pulsations can be determined based on long-term and high-precision photometric observations of such stars, which can constrain the stellar evolutionary phase of the star (e.g. Yang, Fu & Zha 2012).

The star AE Ursae Majoris (hereafter AE UMa = HIP 47181, $\alpha_{2000} = 09^h36^m53^s$, $\delta_{2000} = 44°04'01''$, $\langle V \rangle = 11.27$ mag, $P_0 = 0.0860$ d, $\Delta V = 0.10$ mag) was discovered to be a variable star by Geyer, Kippenhahn & Strohmeier (1955). The spectral type of AE UMa was classified in accordance with the type of variability by Götz & Wenzel (1961) as A9. The period of light variations was determined by Tsesevich (1973), and they classified it as a dwarf Cepheid. The beat phenomenon of the pulsations of this star was found by Szeidl (1974). AE UMa was listed as an SX Phe star by Garcia et al. (1995). However, Hintz, Hintz & Joner (1997b) showed strong evidence against this classification and reclassified it as a normal Population I HADS. According to the measurement of Breger & Pamyatnykh (1998), AE UMa had a fast period decreasing rate of 4.8×10^{-7} yr^{-1}; hence, it should be a pre-MS star. However, there is no other evidence for this star to be a pre-MS star. Recently, both Pócs & Szeidl (2001) and Zhou (2001) analysed pulsations of the star with high-precision and longer photometric data. Their results are consistent with the outcomes of Hintz et al. (1997b): AE UMa is a Population I, post-MS δ Scuti star, but with a stable fundamental frequency and the first overtone decreasing with a rate of $\sim 10^{-8}$ yr^{-1}.

In this paper, we present a detailed study of the pulsations and the period changes of AE UMa, mainly based on both photometric observations and spectroscopic observations. Based on the observational results, we perform theoretical explorations using the stellar code MESA and constrain the physical parameters on this star. The organization of the paper is as follows: Section 2 describes the photometry and data reduction, as well as spectral results; we present the pulsation analysis of the new data in Section 3; in Section 4, the rate of period change of the fundamental pulsations is determined before we conduct calculations of the stellar models with the constraints of the stellar parameters, the frequencies and their variations in Section 5. The conclusions of this study is given in the final section.

2 OBSERVATIONS AND DATA REDUCTION

Photometric observations for AE UMa were made with the 85-cm telescope located at the Xinglong Station of NAOC between 2009

Table 2. The comparison star and the check star used in the photometry of AE UMa.

Star name	$\alpha(2000)$	$\delta(2000)$	V	B	$B-V$
Object = AE Ursae Majoris	$09^h36^m53\overset{s}{.}155$	$+44°04'00\overset{''}{.}39$	11.35 ± 0.08	11.54 ± 0.06	0.19 ± 0.14
Comparison = TYC 2998-1249-1	$09^h37^m28\overset{s}{.}5826$	$+44°01'16\overset{''}{.}854$	11.32 ± 0.08	11.82 ± 0.08	0.50 ± 0.16
Check = TYC 2998-1166-1	$09^h37^m12\overset{s}{.}058$	$+43°58'20\overset{''}{.}12$	12.21 ± 0.18	13.10 ± 0.30	0.89 ± 0.48

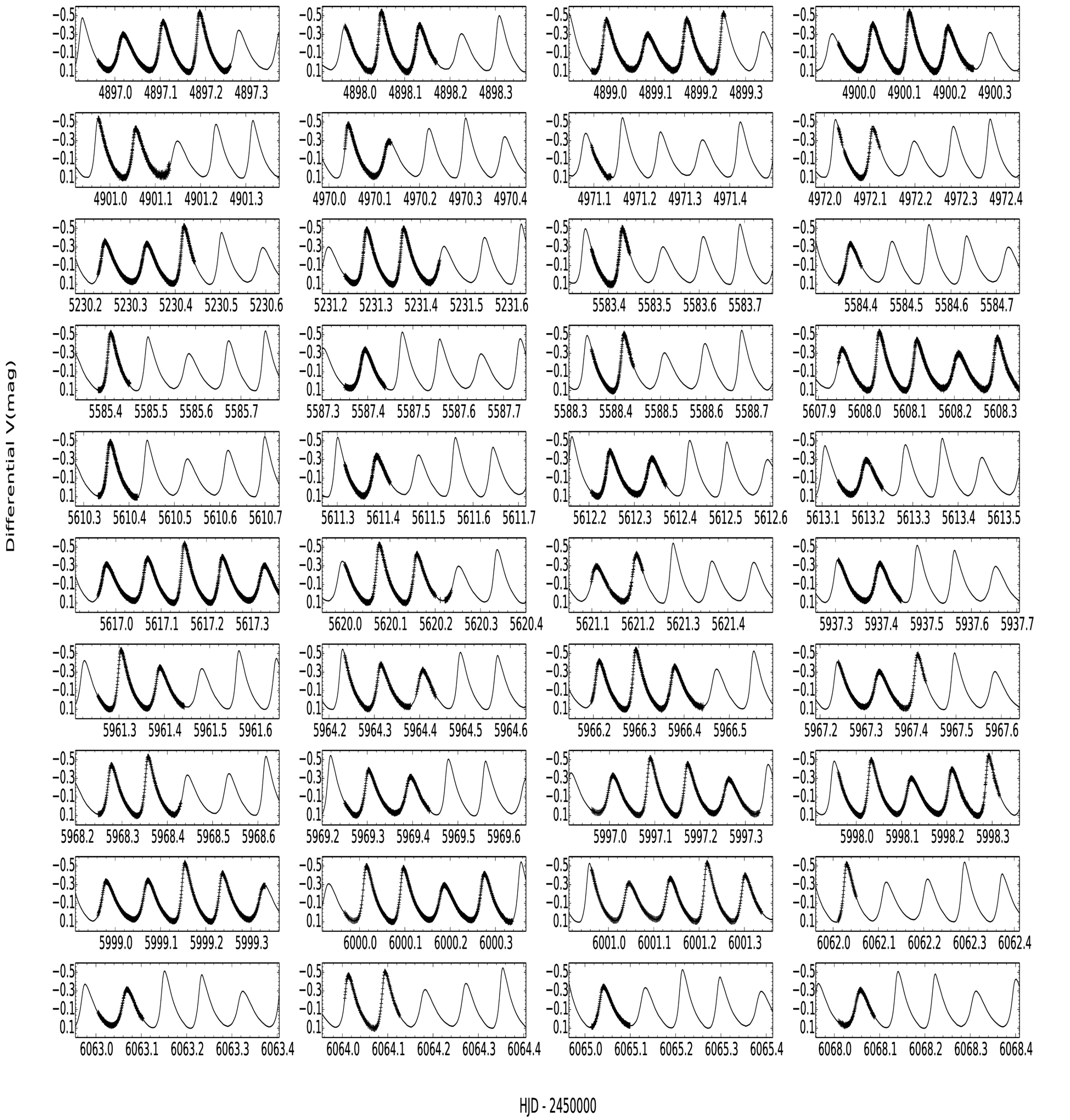

Figure 2. Light curves of AE UMa relative to the comparison star in the V band from 2009 to 2012, observed with the 85-cm telescope. The solid curves represent the fitting with a solution up to 18 frequencies listed in Table 3.

March and 2012 May. The 85-cm telescope was equipped with a standard Johnson–Cousin–Bessel multicolour filter system and a PI1024 BFT CCD camera mounted on the primary focus (Zhou et al. 2009). The CCD had 1024 × 1024 pixels, corresponding to a field of view of 16.5 × 16.5 arcmin^2. Since 2012 March, the CCD camera has been replaced by a PI512 BFT with a larger size of pixels, which has 512 × 512 pixels corresponding to a field of view of 15 × 15 arcmin^2. The observations were made through a

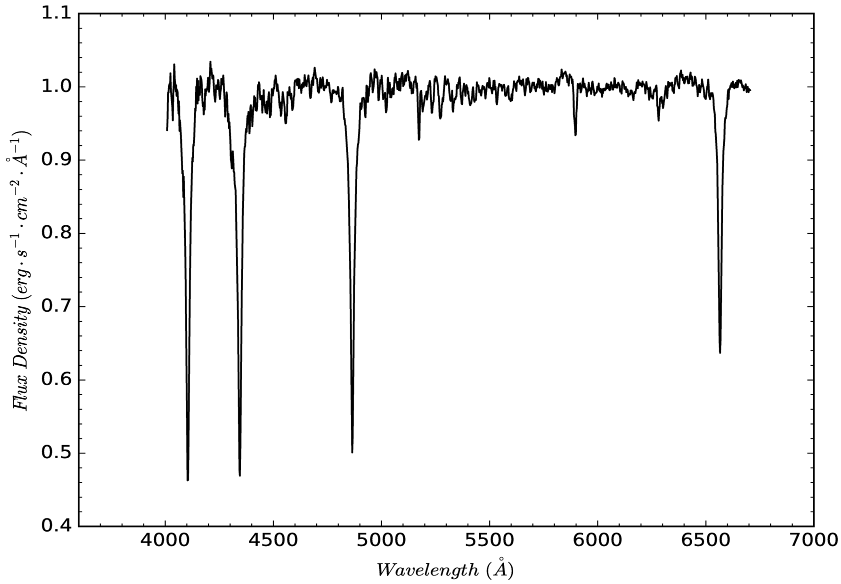

Figure 3. Spectroscopic observation results of AE UMa.

Table 3. Parameters of AE UMa derived from spectroscopic observations.

Parameters	Values	σ
$T_{\rm eff}$ (K)	7600	180
$\log g$	4.1	0.2
[Fe/H]	−0.32	0.23
RV (km s^{-1})	150	27

standard Johnson V filter with the exposure time ranging from 15 to 120 s, depending on the atmospheric conditions. A journal of the new observations is listed in Table 1.

In total, 17 277 CCD frames were collected for AE UMa during 40 nights. Fig. 1 shows an image of AE UMa taken with the 85-cm telescope, where the comparison star (TYC 2998-1249-1) and the check star (TYC 2998-1166-1) are marked as well. The details of the three stars from SIMBAD (Wenger et al. 2000) are listed in Table 2.

The preliminary processing of the CCD frames (bias, dark subtraction and flat-field correction) was performed with the standard routines of CCDPROC from the IRAF software. After that, we employed the IRAF DAOPHOT package to perform aperture photometry. In order to optimize the size of the aperture, we used 12 different sizes of apertures for the data in each night and adopted the aperture that brought the minimum variance of the magnitude differences between the check star and the comparison star. The data reduction was carried out with the standard process of aperture photometry.

The light curves were then produced by computing the magnitude differences between AE UMa and the comparison star. The standard deviations of the magnitude differences between the check star and the comparison star yielded an estimation of photometry precisions, with a typical value of 0.003 mag in good observation conditions and 0.011 mag in poor cases from night to night. As there were slight zero-point shifts, we adjusted it with the fitted light curves for every month by assuming that the pulsations were stable in one month.

Fig. 2 shows the light curves of AE UMa in the Johnson V band observed with the 85-cm telescope in 2009–2012, which was used to conduct pulsation analysis, and determination of new times of maximum light.

Spectroscopic observations of AE UMa were made with the 2.16-m telescope, which is located at the Xinglong station of NAOC, on 2016 May 21. The BFOSC low-dispersion spectrometer was employed for the observations. The used grating was G7 with a slit width of 1.8 arcsec and a line dispersion of 95 Å mm^{-1}. The centre wavelength was at 530 nm with the wavelength range of 380–680 nm.

The data were reduced with IRAF, and the obtained low-resolution spectrum is shown in Fig. 3. With the results from spectroscopic observations, we used the automated 1D parametrization pipeline LASP, which is based on the stellar spectral template library (Wu et al. 2011), to get the stellar atmospheric parameters (see Table 3). We note that $T_{\rm eff}$ and $\log g$ correspond to a fixed phase since we had acquired only one spectrum. These values may vary differently from phase to phase during the pulsations of AE UMa. However, the metal-to-hydrogen ratio [Fe/H] is not sensitive to the pulsations. The value of [Fe/H] is $-0.32(\pm 0.23)$, which indicates that AE UMa is possibly a Population I δ Scuti star. This is consistent with the classification of the results obtained from Hintz et al. (1997b), Pócs & Szeidl (2001) and Zhou (2001) without spectroscopic data. Hence, AE UMa can be modelled as a single star in Section 5.

3 PULSATION ANALYSIS

Pulsation analysis was performed with the light curves of AE UMa in the years 2009–2012, respectively, with the software PERIOD04 (Lenz & Breger 2005), which provides Fourier transformations of the light curves to search for significant peaks in the amplitude spectra until 150 c d^{-1}, since there are no significant peaks above this frequency limit. Then, the light curves are fitted with the following formula:

$$m = m_0 + \Sigma A_i \sin(2\pi(f_i t + \phi_i)). \tag{1}$$

Table 4 lists the solutions of 37 frequencies whose signal-to-noise ratios (S/N) are higher than 4.0 (Breger et al. 1993), and the averaged noise level is calculated over the whole frequency range of 0–150 c d^{-1} (e.g. Kepler et al. 2005). The solid curves in Fig. 2

Table 4. Multifrequency solutions of the light curves of AE UMa in the V band in 2009–2012. Fre: Frequency in c d^{-1}. Amp: Amplitude in mmag. S/N: signal-to-noise ratio.

NO.	Marks	Fre	Amp 2009	SN	Fre	Amp 2010	SN	Fre	Amp 2011	SN	Fre	Amp 2012	SN
1	f_0	11.625 25	220.45	1078.98	11.629 44	216.36	2343.67	11.625 49	218.93	1360.27	11.625 58	218.26	1652.90
2	$2f_0$	23.250 14	74.36	373.67	23.258 88	73.25	727.33	23.250 36	73.77	467.10	23.251 08	73.57	565.07
3	f_1	15.031 09	45.29	223.73	15.011 05	43.95	464.85	15.032 01	45.00	278.92	15.031 17	45.11	343.71
4	$3f_0$	34.878 73	28.48	147.81	34.888 32	29.66	299.18	34.876 20	27.70	175.13	34.876 80	27.99	216.03
5	f_0+f_1	26.658 47	29.39	148.03	26.640 49	28.76	294.84	26.656 20	29.27	184.42	26.656 65	29.72	228.20
6	f_1-f_0	3.405 80	25.47	123.84	3.422 85	27.36	282.12	3.406 60	24.36	153.48	3.405 72	25.44	192.97
7	$2f_0+f_1$	38.282 17	16.24	84.60	39.342 15	15.07	150.52	38.282 80	16.11	101.50	38.282 16	15.97	123.94
8	$4f_0$	46.512 74	12.80	67.53	46.559 00	13.02	126.33	46.501 60	12.91	82.28	46.502 33	12.99	100.78
9	$3f_0+f_1$	49.907 05	9.31	49.30	49.940 62	10.26	97.83	49.908 20	9.14	57.64	49.907 96	9.11	71.07
10	$5f_0$	58.134 93	6.23	33.19	57.157 47	4.19	37.35	58.127 00	5.89	36.99	58.127 68	5.99	47.29
11	$2f_0-f_1$	8.227 89	6.16	29.75	9.155 09	6.12	66.30	8.222 57	6.44	40.27	8.218 96	6.21	46.75
12	$4f_0+f_1$	61.541 23	4.99	26.63	60.332 88	5.85	50.38	61.533 60	5.15	31.85	61.534 27	4.92	38.89
13	f_0+2f_1	41.703 15	4.33	22.78	41.775 26	3.15	31.22	41.689 40	4.16	26.42	41.688 53	4.22	32.67
14	$2f_1$	30.080 96	3.77	19.17	30.063 34	5.03	50.90	30.064 00	3.32	20.86	30.061 74	4.00	30.82
15	$6f_0$	69.769 12	3.68	19.56	69.859 13	3.51	28.13	69.752 40	3.74	23.61	69.753 22	3.29	26.59
16	$2f_1-f_0$	19.814 09	3.45	17.17	18.227 71	3.46	36.34	19.844 20	3.04	19.00	19.845 74	3.16	24.26
17	$5f_0+f_1$	73.163 42	3.27	17.40	74.230 48	3.31	25.21	73.159 00	3.31	20.83	73.159 80	3.42	27.88
18	$6f_0+f_1$	84.763 12	2.15	11.31	84.773 68	2.83	19.70	84.782 67	2.21	14.30	84.785 66	2.19	18.38
19	$2f_0+2f_1$	53.349 33	2.07	11.00	53.693 38	1.82	16.55	53.314 80	1.66	10.51	53.312 82	2.26	17.81
20	$7f_0$	81.392 80	2.00	10.53	80.567 29	1.80	12.95	81.379 84	1.90	12.21	81.380 32	1.93	15.96
21	$7f_0+f_1$	96.397 30	1.45	7.94	96.361 88	1.51	9.96	96.408 07	1.60	10.48	96.411 20	1.62	14.13
22	$3f_0+2f_1$	64.935 53	1.60	8.59	63.838 21	3.22	26.65	64.943 97	1.64	10.21	64.938 35	1.59	12.67
23	$4f_0-f_1$	31.448 28	1.76	9.02	31.547 95	1.18	11.96	32.242 12	1.34	8.43	31.470 03	1.56	12.05
24	$2f_1-2f_0$	6.776 61	1.41	6.81	7.794 20	3.97	42.67	6.025 61	2.05	12.85	7.788 61	1.07	8.06
25	$2f_1-f_0$	18.458 77	1.40	6.98	18.227 71	3.46	36.34	18.442 37	2.04	12.70	18.437 45	1.93	14.83
26	$4f_0+2f_1$	76.547 23	1.32	7.07	–	–	–	75.798 89	1.16	7.32	76.562 96	1.18	9.64
27	$8f_0+f_1$	108.007 50	1.06	5.94	109.104 78	1.26	7.68	108.033 47	1.25	8.15	108.035 49	0.99	8.77
28	$8f_0$	93.038 98	1.22	6.65	–	–	–	93.012 78	0.88	5.75	93.005 86	1.18	10.13
29	$5f_0+2f_1$	88.205 40	1.05	5.55	–	–	–	88.185 50	1.06	6.91	88.189 75	1.05	8.95
30	$6f_0-f_1$	54.692 65	1.20	6.36	–	–	–	53.314 80	1.66	10.51	54.724 85	0.98	7.74
31	$3f_1$	44.053 97	1.03	5.45	–	–	–	43.098 77	1.13	7.24	43.096 81	1.00	7.75
32	$10f_0+f_1$	131.287 86	0.91	5.43	–	–	–	–	–	–	–	–	–
33	$9f_0+f_1$	119.629 69	0.82	4.78	118.713 50	0.97	5.63	119.655 10	0.72	4.76	118.655 64	0.57	4.97
34	$6f_0+2f_1$	100.823 09	0.78	4.35	100.774 47	0.99	6.34	99.814 67	1.01	6.64	99.815 28	0.77	6.75
35	$7f_0+2f_1$	110.502 25	0.73	4.16	110.995 41	0.78	7.68	111.439 57	0.69	5.19	–	–	–
36	$9f_0$	103.665 67	0.71	4.01	104.898 39	0.90	5.74	104.864 28	0.69	4.48	103.653 46	0.67	5.94
37	$8f_0+2f_1$	–	–	–	–	–	–	–	–	–	123.067 60	0.54	4.82

show the fits with the frequency solutions in different years. From Table 4, one notes that the 37 frequencies are composed of the fundamental and the first overtone frequencies, their harmonics and linear combinations. As can be noted, no significant signals are detected in addition to these frequencies.

Figs 4 and 5 show, respectively, the window function and the amplitude spectra of the frequency pre-whitening process for the light curves in V in 2009.

As can be seen from Fig. 2, the constructed curves fit well the light curves observed in 2009–2012, respectively, which shows that the fundamental and the first overtone frequencies, together with their harmonics and linear combinations, can explain the pulsation behaviour of AE UMa.

To show the variations of the frequencies and amplitudes of pulsations of the star, we compare our results with those from Zhou (2001), who analysed the data for AE UMa from 1974 to 2001. By dividing the data into four segments of data sets following Zhou (2001), we resolved the pulsation parameters of the fundamental and the first overtone frequencies of AE UMa and listed them in Table 5.

4 THE O − C DIAGRAM

With the new observations from 2009 to 2012, the light curves around the light maxima were fitted with a fourth polynomial by the non-linear least-squares method. The errors in polynomial fitting are consistent with the uncertainties estimated from Monte Carlo simulations of 100 iterations for each maximum. We obtained 84 times of maximum light in the V band, as listed in Table 6.

In order to conduct an O − C analysis for the period change of AE UMa, we combined the new times of maximum light with those provided from the previous literature.[1] We finally obtained 461 times of maximum light, which are listed in Table 7. We discarded 17 times of maximum light, which were collected with either photograph

[1] Agerer, Dahm & Hubscher (1999a), Pócs & Szeidl (2001), Pejcha, Havlik & Kral (2001), Zhou (2001), Agerer & Hubscher (2003), Hubscher (2005), Hubscher, Paschke & Walter (2005), Klingenberg, Dvorak & Robertson (2006), Hubscher, Paschke & Walter (2006), Hubscher & Walter (2007), Samolyk (2010), Hubscher (2007), Hubscher, Steinbach & Walter (2009), Hubscher et al. (2010) and Huebscher & Monninger (2011).

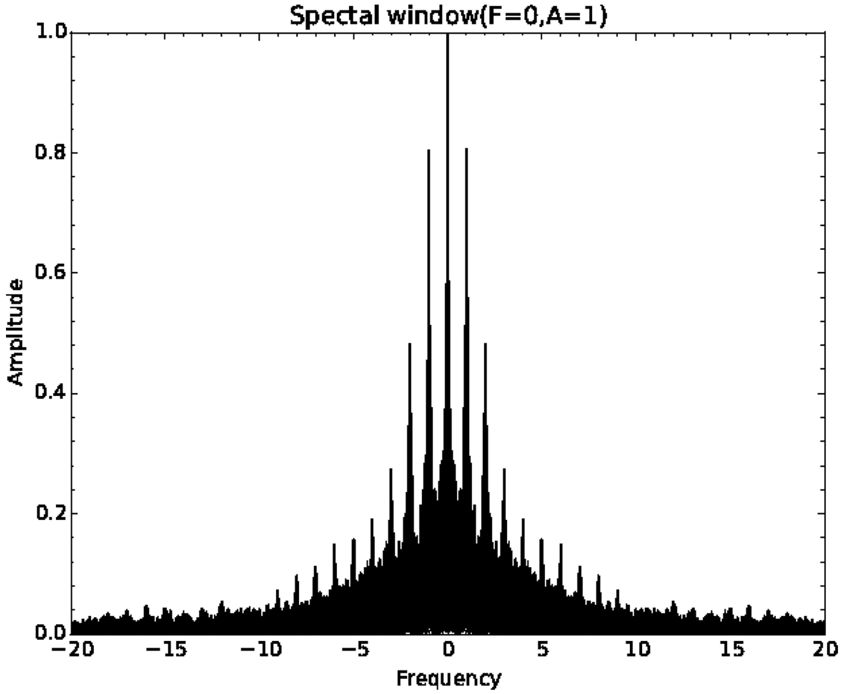

Figure 4. Spectral window of the light curves in V for AE UMa in 2009.

(pg) or visual (vis), with large uncertainties, compared to those collected with the CCD or photoelectric photometer (pe). We finally used 444 data points to construct the O − C (the Observed minus Calculated values) diagram. The used linear ephemeris formula is

$$\mathrm{HJD}_{\max} = 2442062.5824 + 0\overset{\mathrm{d}}{.}08601707\,E \tag{2}$$

following Pócs & Szeidl (2001).

A linear fit to the 444 times of maximum light yields the ephemeris formula

$$\begin{aligned}\mathrm{HJD}_{\max} = {} & 2442062.5818(\pm 0.0002) \\ & + 0\overset{\mathrm{d}}{.}086017078(\pm 0.000000002)E\end{aligned} \tag{3}$$

with a standard deviation of $\sigma_0 = 0.002\,46$ d. The O − C values are listed in Table 7 as well. The O − C diagram is shown in Fig. 6.

In addition, we made a quadratic fit with a second-order polynomial:

$$\begin{aligned}\mathrm{HJD}_{\max} = {} & 2442062.5822(\pm 0.0002) \\ & + 0.086017060(\pm 0.000000006)E \\ & + 0.5 \times 1.09(\pm 0.38) \times 10^{-13} E^2\end{aligned} \tag{4}$$

with the standard deviation of $\sigma_1 = 0.002\,44$ d. The quadratic terms differ from zero by a factor of 2.87σ with a significance of ∼99.5 per cent, and the statistic test proposed by Pringle (1975) suggests that the small improvement in period deviation gives the quadratic term in the fit with a significance of ∼99.3 per cent. From the values in equation (4), we take the period change rate of AE UMa as $(1/P_0)(\mathrm{d}P_0/\mathrm{d}t) = 5.4(\pm 1.9) \times 10^{-9}\ \mathrm{yr}^{-1}$, which is different from the result of $-0.35 \times 10^{-10}\ \mathrm{yr}^{-1}$ provided by Zhou (2001). This value will be used in our model calculations in the next section. However, the data may not be distributed as Gaussian random noise, and more data points need to be collected to confirm this period change.

Since the modulation frequency $f_\mathrm{m} = f_1 - f_0$ has not been varying significantly compared with f_1 (Pócs & Szeidl 2001), one may take the method that is used in Pócs & Szeidl (2001) and Zhou (2001) to calculate the rate of changes of the first overtone frequency. But the result shows large uncertainties. Hence, we do not consider it a credible result from our observations.

5 CONSTRAINTS FROM THE THEORETICAL MODELS

Because the order of the period change of the fundamental mode is the same as the result from our calculation in Section 4 in the post-MS phase (about $10^{-8}\ \mathrm{yr}^{-1}$), we assume that the result is completely from the evolutionary effects.

In this section, we describe the details of the calculation of the theoretical models of AE UMa to constrain the physical parameters for the target. Section 5.1 presents the initial input physical parameters of AE UMa for the theoretical models; Section 5.2 uses the two frequencies f_0 and f_1 to constrain the initial parameters and determines some parameters for the subsequent calculation; Section 5.3 uses two independent ways to calculate the period changes of the fundamental mode of AE UMa induced by the stellar evolutionary effects.

5.1 Physical parameters

Rodriguez et al. (1992) conducted $uvby\beta$ photoelectric photometry for AE UMa. Intrinsic values of $b - y$, m_1 and c_1 were derived and the stellar physical parameters were determined. The effective temperature of AE UMa varied from 8320 to 7150 K. The surface gravity $\log g$ varied from 4.16 to 3.77. The mean values obtained along the cycle were $\langle T_\mathrm{eff}\rangle = 7560$ K and $\langle \log g\rangle = 3.90$, respectively. The metal abundance was estimated from δm_1 at the minimum light as [Fe/H] = −0.3. By using the $\log g$–$\log P$ relation derived by Claret et al. (1990), Rodriguez et al. (1992) obtained the values of $M = 1.80\,\mathrm{M}_\odot$, age $= 1.3 \times 10^9$ yr and $M_\mathrm{bol} = 1.76$ mag. Hintz et al. (1997b) provided the value of [Fe/H] = −0.1 according

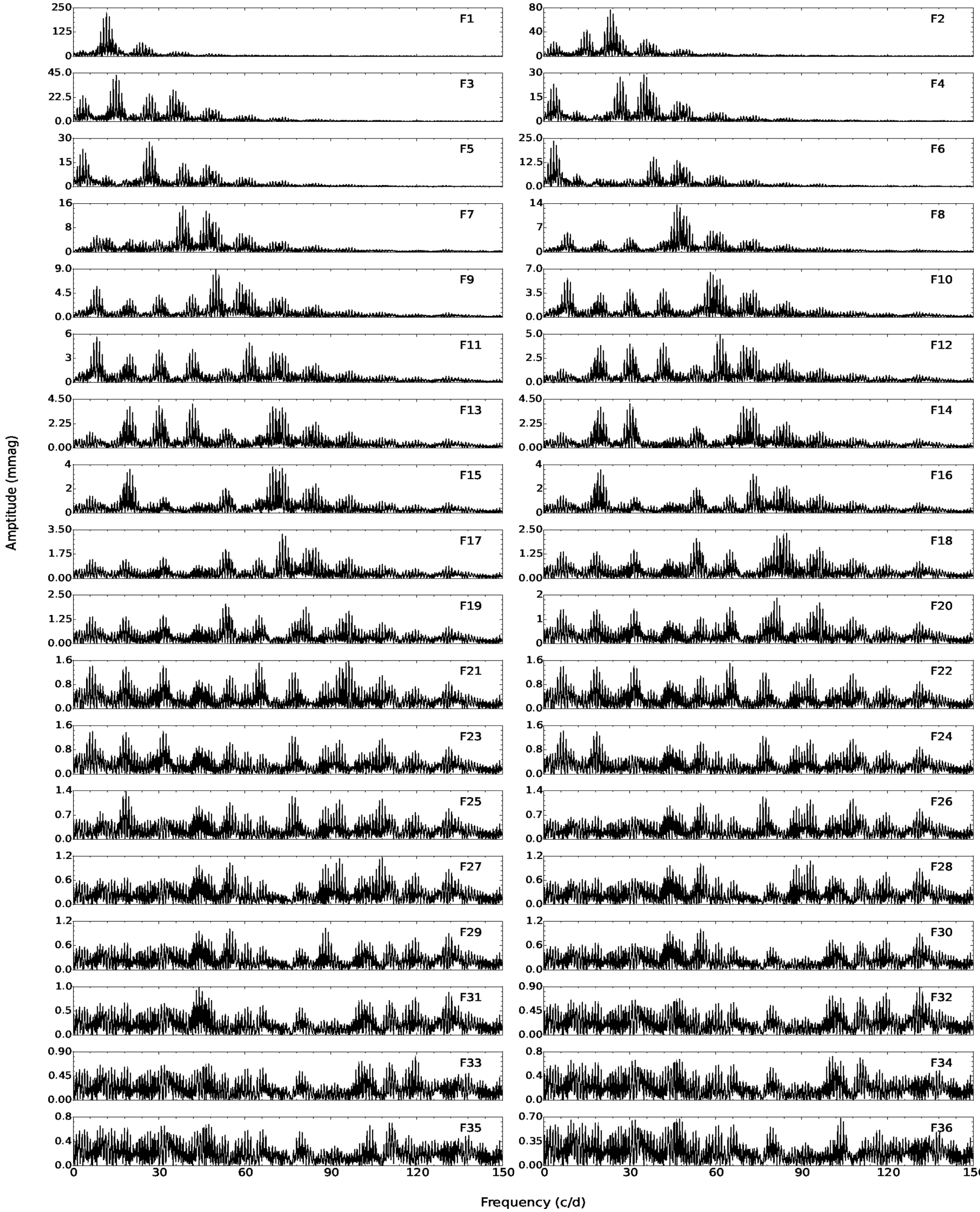

Figure 5. Amplitude spectrum of the light curves in *V* for AE UMa collected in 2009, and the amplitude spectra of the frequency pre-whitening process. Note that the *y*-axis scales are optimized concerning the highest peaks in the panels.

to the relation between the P_1/P_0 ratio and the [Fe/H] value for dwarf Cepheids, which was derived from Hintz et al. (1997a). They got the [Fe/H] values ranging from −0.4 to −0.1. We listed the parameters of AE UMa from Rodriguez et al. (1992) and Hintz et al. (1997b) in Table 8. The atmospheric parameters derived from our spectrum are in good agreement with the above values, in particular, for the metal ratio [Fe/H] (comparison of Table 3 to 11). We note that in order to perform a search for the best-fitting model in a wide

Table 5. Frequencies and amplitudes of AE UMa for different segments of observations, including the data sets of Zhou (2001) and our data. (The data of 1981–1987 have not been used due to their large scatters.)

Years	f_0	f_1	A_0	A_1
1974–1977	11.625 57	15.030 97	216.9	34.1
⋆1981–1987	11.622 90	15.072 59	219.6	29.4
1996–1998	11.625 60	15.031 22	210.9	36.8
2000–2001	11.625 61	15.031 19	207.0	38.6
2009–2012	11.625 60	15.031 23	219.0	45.1
Mean	11.625 60	15.031 20	213.5	38.7
σ	0.000 015	0.000 123	5.5	4.7

Table 6. Newly determined times of maximum light of AE UMa. $T_{\max}$ is in HJD − 2450000. σ is the estimated uncertainty of the times of maximum light in days.

$T_{\max}$	σ	$T_{\max}$	σ
4897.018 76	0.000 09	5621.110 32	0.000 17
4897.106 88	0.000 08	5621.198 60	0.000 19
4897.188 28	0.000 04	5937.398 14	0.000 12
4898.048 97	0.000 10	5961.305 07	0.000 04
4898.133 12	0.000 15	5961.390 70	0.000 10
4898.993 05	0.000 13	5964.314 79	0.000 14
4899.083 69	0.000 23	5964.40728	0.000 19
4899.170 58	0.000 13	5966.213 31	0.000 07
4900.031 82	0.000 10	5966.294 16	0.000 05
4900.112 85	0.000 08	5966.379 65	0.000 08
4900.197 79	0.000 14	5967.331 06	0.00 009
4901.057 55	0.000 27	5967.415 92	0.000 07
4970.043 14	0.000 08	5968.277 34	0.000 07
4972.107 76	0.000 24	5968.358 17	0.000 04
5230.245 53	0.000 09	5969.303 81	0.000 07
5230.33788	0.000 10	5969.395 94	0.000 14
5230.420 07	0.000 08	5997.008 00	0.000 08
5231.281 78	0.000 08	5997.090 64	0.000 04
5231.363 52	0.000 06	5997.172 95	0.000 04
5583.431 32	0.000 12	5997.263 91	0.000 10
5584.378 69	0.00018	5998.033 73	0.000 08
5585.413 21	0.000 08	5998.122 09	0.000 14
5587.394 57	0.000 09	5998.211 92	0.000 08
5588.420 08	0.000 08	5998.292 74	0.000 06
5607.952 82	0.000 18	5998.980 78	0.000 09
5608.034 84	0.000 11	5999.072 67	0.000 09
5608.118 00	0.000 11	5999.154 66	0.000 05
5608.209 86	0.000 22	5999.237 46	0.000 05
5608.295 35	0.000 12	6000.016 12	0.000 05
5608.376 32	0.000 11	6000.097 80	0.000 04
5610.359 12	0.000 10	6000.187 42	0.000 09
5611.387 74	0.000 16	6000.276 18	0.000 06
5612.246 92	0.000 14	6001.045 94	0.000 06
5612.339 17	0.000 22	6001.136 82	0.000 06
5613.197 99	0.000 21	6001.2185 7	0.000 03
5616.980 03	0.000 11	6001.302 28	0.000 06
5617.070 53	0.000 08	6062.031 20	0.000 05
5617.151 98	0.000 05	6063.069 10	0.000 15
5617.235 83	0.000 06	6064.013 67	0.000 08
5617.328 10	0.000 10	6064.094 79	0.000 08
5620.077 17	0.000 10	6065.041 89	0.000 09
5620.160 24	0.000 17	6068.057 99	0.000 21

parametric range, we used 3σ as the intervals of constraints for our theoretical calculation as follows.

5.2 Constraints from f_0 and f_1

MESA is a suite of open-source, robust, efficient, thread-safe libraries for a wide range of applications in computational stellar astrophysics (Paxton et al. 2011, 2013). The 1D stellar evolution module, MESA star, combines many of the numerical and physics modules for simulations of a wide range of stellar evolution scenarios ranging from very low mass to massive stars, including advanced evolutionary phases. The '*astero*' extension to the MESA star implements an integrated approach that passes results automatically between the MESA star and the new MESA module based on the adiabatic code ADIPLS (Christensen-Dalsgaard 2008).

In MESA version 6208, the *astero* extension enables the calculation of selected pulsation frequencies by the MESA star during the evolution of the model. This allows fitting to the observations that can include spectroscopic constraints (e.g. [Fe/H], $\log g$ and $T_{\rm eff}$), asteroseismic constraints, a large frequency separation ($\Delta\nu$) and the frequency of maximum power ($\nu_{\max}$), and even individual frequencies observed. For the automated χ^2 minimization, *astero* will evolve a pre-MS model from a user-defined starting point, and find the best match along that single evolutionary track. The code then recalculates the track, again initiated at the pre-MS, with different initial parameters such as mass, chemical composition, mixing-length parameter and overshooting, and repeats until the minimum χ^2 is found.

We used the scan-grid mode to minimize the χ^2 for each model, which helps to compact the intervals of the physical parameters.

Every model of evolution starts with creating a pre-MS model by specifying the mass, M, at a uniform composition. The equation-of-state tables are constructed from the 2005 update of the OPAL EOS (Rogers & Nayfonov 2002) and SCVH tables (Saumon, Chabrier & van Horn 1995). The MESA opacity tables, which are derived from Type 1 and 2 OPAL tables (Iglesias & Rogers 1993, 1996), and tables from OP (Seaton 2005; Ferguson et al. 2005), cover a large range of $2.7 \le \log T \le 10.3$ and $-8 \le \log R \le 8$. The hydrogen burning reaction rates in the calculations are from Bahcall (1997, 2002).

The MESA star treats convective mixing as a time-dependent, diffusive process with a diffusion coefficient $D_{\rm OV}$ defined as

$$D_{\rm OV} = D_{\rm conv,0} \exp\left(-\frac{2z}{f\lambda_{\rm P,0}}\right), \tag{5}$$

where $\lambda_{\rm P,0}$ is the pressure scaleheight at that location, z is the distance in the radiative layer away from that location and f is an adjustable parameter (Herwig 2000).

In all our subsequent calculations, the used opacity and EOS tables are $eos\_file\_prefix = mesa$, $kappa\_file\_prefix = gs98$ and $kappa\_lowT\_prefix = lowT\_Freedman11$. The atmosphere model is the $which\_atm\_option = photosphere\_tables$ photosphere.

The mixing-length parameter $\alpha_{\rm MLT}$ was chosen as 1.89, since the choice has actually a very small effect on our models (Yang et al. 2012). The convective overshooting parameter $f_{\rm ov} = 0.015$ was the initial value of MESA (version 6208). The effects of rotation on the evolutionary period changes are disregarded, concerning AE UMa as an HADS with very slow rotation (Breger 2000). Table 9 lists the parameters of the grid of model to search for f_0 and f_1 of AE UMa. The diffusion effects were not taken into account because of its negligible results on the models with mass in the range of

Table 7. Times of maximum light and O − C values of AE UMa. T_{max} is the observed times of maximum light in HJD − 2400000. E: cycle number. O − C is in days. Det: detector (pg = photograph, vis = visual, and pe = photoelectric photometer). S: source [(1) Tsesevich (1973); (2) Filatov (1960); (3) Pócs & Szeidl (2001); (4) Broglia & Conconi (1975); (5) Braune, Huebscher & Mundry (1979); (6) Braune & Mundry (1982); (7) Huebscher, Lichtenknecker & Mundry (1985); (8) Rodriguez et al. (1992); (9) Hübscher, Agerer & Wunder (1992); (10) Hintz et al. (1997b); (11) Agerer, Dahm & Hubscher (1999b); (12) Agerer et al. (1999a); (13) Pejcha et al. (2001); (14) Zhou (2001); (15) Agerer & Hubscher (2003); (16) Hubscher (2005); (17) Hubscher et al. (2005); (18) Klingenberg et al. (2006); (19) Hubscher et al. (2006); (20) Hubscher & Walter (2007); (21) Samolyk (2010); (22) Hubscher (2007); (23) Hubscher et al. (2009); (24) Hubscher et al. (2010); (25) Huebscher & Monninger (2011); and (26) this work.]. Points not used in the O − C analysis are marked with an asterisk.

NO.	T_{max}	E	O − C	Det	S	NO.	T_{max}	E	O − C	Det	S
1	28 632.398	−156 133	–	pg	(1)*	58	43 162.5708	12 788	0.002 457	pe	(3)
2	31 875.122	−118 434	–	pg	(2)*	59	44 633.4626	29 888	0.002 451	pe	(3)
3	33 379.256	−100 948	–	pg	(2)*	60	44 633.5440	29 889	−0.002 166	pe	(3)
4	35 601.188	−75 117	–	pg	(2)*	61	44 633.6309	29 890	−0.001 283	pe	(3)
5	35 604.337	−75 080	–	vis	(1)*	62	44 634.4046	29 899	−0.001 737	pe	(3)
6	35 607.173	−75 047	–	pg	(2)*	63	44 634.4902	29 900	−0.002 154	pe	(3)
7	35 981.202	−70 699	–	pg	(2)*	64	44 634.5810	29 901	0.002 629	pe	(3)
8	38 106.402	−45 992	–	vis	(1)*	65	44 692.4709	30 574	0.003 043	pe	(3)
9	41 059.368	−11 662	–	vis	(1)*	66	44 696.343	30 619	–	vis	(6)*
10	41 773.223	−3363	–	vis	(1)*	67	44 696.426	30 620	–	vis	(6)*
11	42 062.5832	0	0.001 039	pe	(3)	68	44 696.520	30 621	–	vis	(6)*
12	42 065.5959	35	0.003 142	pe	(4)	69	45 355.4902	38 282	0.002 786	pe	(3)
13	42 065.6778	36	−0.000 975	pe	(4)	70	45 355.5727	38 283	−0.000 731	pe	(3)
14	42 068.3432	67	−0.002 104	pe	(4)	71	45 382.3228	38 594	−0.001 939	pe	(3)
15	42 068.4302	68	−0.001 121	pe	(4)	72	45 382.4104	38 595	−0.000 356	pe	(3)
16	42 068.5203	69	0.002 962	pe	(4)	73	45 382.4997	38 596	0.002 927	pe	(3)
17	42 068.6029	70	−0.000 455	pe	(4)	74	45 382.5807	38 597	−0.002 090	pe	(3)
18	42 068.6871	71	−0.002 272	pe	(4)	75	46 114.332	47 104	–	vis	(7)*
19	42 069.3808	79	0.003 292	pe	(4)	76	46 468.4601	51 221	−0.002 180	pe	(3)
20	42 069.4651	80	0.001 574	pe	(4)	77	46 468.5468	51 222	−0.001 497	pe	(3)
21	42 069.5473	81	−0.002 243	pe	(4)	78	46 855.6279	55 722	0.002 780	pe	(8)
22	42 069.6363	82	0.000 740	pe	(4)	79	46 856.5729	55 733	0.001 592	pe	(8)
23	42 086.4965	278	0.001 597	pe	(4)	80	46 856.6561	55 734	−0.001 225	pe	(8)
24	42 086.5787	279	−0.002 221	pe	(4)	81	46 857.6017	55 745	−0.001 812	pe	(8)
25	42 087.4390	289	−0.002 091	pe	(4)	82	46 857.6925	55 746	0.002 970	pe	(8)
26	42 087.5263	290	−0.000 808	pe	(4)	83	46 858.6382	55 757	0.002 483	pe	(8)
27	42 087.6155	291	0.002 375	pe	(4)	84	46 859.6666	55 769	−0.001 322	pe	(8)
28	42 095.5298	383	0.003 105	pe	(3)	85	46 878.4181	55 987	−0.001 544	pe	(8)
29	42 095.6123	384	−0.000 412	pe	(3)	86	46 878.5064	55 988	0.000 739	pe	(8)
30	42 103.3513	474	−0.002 947	pe	(4)	87	46 878.5946	55 989	0.002 922	pe	(8)
31	42 106.4523	510	0.001 439	pe	(3)	88	46 884.5262	56 058	−0.000 656	pe	(8)
32	42 119.5252	662	−0.000 255	pe	(3)	89	46 884.6117	56 059	−0.001 173	pe	(8)
33	42 121.5025	685	−0.001 347	pe	(3)	90	46 886.5907	56 082	−0.000 566	pe	(8)
34	42 122.3628	695	−0.001 218	pe	(4)	91	48 683.317	76 970	–	vis	(9)*
35	42 122.4484	696	−0.001 635	pe	(4)	92	50 151.4564	94 038	0.000 981	pe	(3)
36	42 128.2968	764	−0.002 395	pe	(3)	93	50 151.5384	94 039	−0.003 036	pe	(3)
37	42 128.3872	765	0.001 988	pe	(3)	94	50 152.3170	94 048	0.001 411	pe	(3)
38	42 128.4727	766	0.001 471	pe	(3)	95	50 152.4862	94 050	−0.001 424	pe	(3)
39	42 128.5557	767	−0.001 546	pe	(3)	96	50 152.5756	94 051	0.001 959	pe	(3)
40	42 133.4627	824	0.002 482	pe	(3)	97	50 458.8815	97 612	0.001 034	CCD	(10)
41	42 133.5442	825	−0.002 035	pe	(3)	98	50 458.9636	97 613	−0.002 883	CCD	(10)
42	42 134.4055	835	−0.000 906	pe	(3)	99	50 459.8240	97 623	−0.002 654	CCD	(10)
43	42 147.3933	986	−0.001 682	pe	(3)	100	50 459.9113	97 624	−0.001 371	CCD	(10)
44	42 148.4295	998	0.002 313	pe	(3)	101	50 467.7388	97 715	−0.001 425	CCD	(10)
45	42 148.5117	999	−0.001 504	pe	(3)	102	50 467.8236	97 716	−0.002 642	CCD	(10)
46	42 159.4365	1126	−0.000 871	pe	(3)	103	50 490.3607	97 978	−0.002 018	pe	(3)
47	42 161.4145	1149	−0.001 263	pe	(3)	104	50 505.6697	98 156	−0.004 058	CCD	(10)
48	42 453.5306	4545	0.000 899	pe	(3)	105	50 505.7595	98 157	−0.000 275	CCD	(10)
49	42 453.6137	4546	−0.002 018	pe	(3)	106	50 505.8461	98 158	0.000 308	CCD	(10)
50	42 460.4989	4626	0.001 817	pe	(3)	107	50 516.7676	98 285	−0.002 362	CCD	(10)
51	42 532.407	5462	–	vis	(5)*	108	50 554.4432	98723	−0.002 243	pe	(3)
52	42 830.6280	8929	−0.000 499	pe	(3)	109	50 813.3550	101 733	−0.001 860	pe	(3)
53	42 837.5120	9009	0.002 136	pe	(3)	110	50 813.4408	101 734	−0.002 077	pe	(3)
54	42 838.4591	9020	0.003 049	pe	(3)	111	50 813.6151	101 736	0.000 189	pe	(3)
55	42 866.496	9346	–	vis	(5)*	112	50 813.6985	101 737	−0.002 428	pe	(3)
56	42 869.3377	9379	0.001 523	pe	(3)	113	50 848.4540	102 141	0.002 170	pe	(3)
57	42 869.4205	9380	−0.001 694	pe	(3)	114	50 848.5391	102 142	0.001 253	pe	(3)

Table 7 – *continued*

NO.	T_{max}	E	O − C	Det	S	NO.	T_{max}	E	O − C	Det	S
115	50 848.6212	102 143	−0.002 664	pe	(3)	179	51 942.2473	114 858	0.002 234	CCD	(14)
116	50 849.4815	102 153	−0.002 535	pe	(3)	180	51 942.3311	114 859	0.000 017	CCD	(14)
117	50 849.5688	102 154	−0.001 252	pe	(3)	181	51 942.4141	119 265	−0.003 000	CCD	(15)
118	50 862.3840	102 303	−0.002 597	CCD	(13)	182	52 321.4089	119 846	0.000 521	CCD	(15)
119	50 862.3840	102 418	−0.002 597	pe	(3)	183	52 371.3836	123 496	−0.000 706	CCD	(15)
120	50 872.2809	102 419	0.002 339	pe	(3)	184	52 685.3460	123 497	−0.000 673	CCD	(15)
121	50 872.3634	102 420	−0.001 178	pe	(3)	185	52 685.4369	124 020	0.004 210	CCD	(15)
122	50 872.4481	102 421	−0.002 496	pe	(3)	186	52 730.4187	124 124	−0.000 926	CCD	(15)
123	50 872.5394	102 733	0.002 787	pe	(3)	187	52 739.3617	124 195	−0.003 703	CCD	(16)
124	50 899.3729	102 734	−0.001 042	pe	(3)	188	52 745.4702	126 928	−0.002 416	CCD	(17)
125	50 899.4570	102 767	−0.002 959	pe	(3)	189	52 980.5608	126 929	0.003 484	CCD	(17)
126	50 902.2976	102 768	−0.000 923	pe	(3)	190	52 980.6421	126 930	−0.001 233	CCD	(17)
127	50 902.3819	102 779	−0.002 640	pe	(3)	191	52 980.7279	127 195	−0.001 451	CCD	(16)
128	50 903.3321	102 780	0.001 372	pe	(3)	192	53 003.5231	127 483	−0.000 779	CCD	(16)
129	50 903.4192	102 781	0.002 455	pe	(3)	193	53028.2942	127 484	−0.002 600	CCD	(16)
130	50 903.5009	107 036	−0.001 862	CCD	(13)	194	53028.3871	127 485	0.004 283	CCD	(16)
131	51 269.5080	107 198	0.002 550	CCD	(13)	195	53028.4705	127 486	0.001 666	CCD	(16)
132	51 283.4410	107 199	0.000 782	CCD	(13)	196	53028.5522	127 487	−0.002 651	CCD	(16)
133	51 283.5250	107 200	−0.001 235	CCD	(13)	197	53028.6420	127 961	0.001 132	CCD	(16)
134	51 283.6090	107 604	−0.003252	CCD	(13)	198	53069.4119	127 962	−0.001 068	CCD	(16)
135	5 1318.3630	107 605	−0.000154	CCD	(13)	199	53069.5029	127 973	0.003 915	CCD	(16)
136	51 318.4460	110 972	−0.003 171	CCD	(14)	200	53070.4493	127 974	0.004 127	CCD	(16)
137	51 608.0716	110 973	0.002 908	CCD	(14)	201	53 070.5320	128 205	0.000 810	CCD	(16)
138	51 608.1577	110 974	0.002 991	CCD	(14)	202	53 090.4053	128 251	0.004 162	CCD	(16)
139	51 608.2395	110 975	−0.00 1226	CCD	(14)	203	53 094.3575	128 437	−0.000 424	CCD	(19)
140	51 608.3264	110 983	−0.000 343	CCD	(14)	204	53 110.3619	131 915	0.004 798	CCD	(18)
141	51 609.0186	110 984	0.003 720	CCD	(14)	205	53 409.5286	131 916	0.004 064	CCD	(18)
142	51 609.1006	110 985	−0.000 297	CCD	(14)	206	53 409.6108	131 917	0.000 247	CCD	(18)
143	51 609.1865	110 986	−0.000 414	CCD	(14)	207	53 409.6940	132 122	−0.002 570	CCD	(19)
144	51 609.2770	110 987	0.004 069	CCD	(14)	208	53 427.3272	132 123	−0.002 873	CCD	(19)
145	51 609.3583	110 995	−0.000 648	CCD	(14)	209	53 427.4181	132 124	0.002 010	CCD	(19)
146	51 610.0450	111 006	−0.002 085	CCD	(14)	210	53 427.5031	132 402	0.000 993	CCD	(17)
147	51 610.9969	111 007	0.003 627	CCD	(14)	211	53 451.4136	132 403	−0.00 1258	CCD	(17)
148	51 611.0821	111 008	0.002 810	CCD	(14)	212	53 451.5042	132 785	0.003 325	CCD	(17)
149	51 611.1627	111 018	−0.002 607	CCD	(14)	213	53 484.3616	136 052	0.002 197	CCD	(20)
150	51 612.0246	111 019	−0.000 878	CCD	(14)	214	53 765.3803	136 053	0.003 066	CCD	(20)
151	51 612.1090	111 020	−0.002 495	CCD	(14)	215	53 765.4660	136 054	0.002 749	CCD	(20)
152	51 612.2010	111 021	0.003 488	CCD	(14)	216	53 765.5462	136 063	−0.003 068	CCD	(20)
153	51 612.2846	111 022	0.001 071	CCD	(14)	217	53 766.3278	136 064	0.004 378	CCD	(20)
154	51 612.3704	111 029	0.000 854	CCD	(14)	218	53 766.4079	136 065	−0.001 539	CCD	(20)
155	51 612.9692	111 030	−0.002 466	CCD	(14)	219	53 766.4943	136 066	−0.001 156	CCD	(20)
156	51 613.0609	111 031	0.003 217	CCD	(14)	220	53766.5849	136 389	0.003 427	CCD	(18)
157	51 613.1453	111 032	0.001 600	CCD	(14)	221	53 794.3619	136 400	−0.003 093	CCD	(18)
158	51 613.2276	111 033	−0.002 117	CCD	(14)	222	53 795.3115	136 401	0.000 319	CCD	(18)
159	51 613.3156	111 053	−0.000 134	CCD	(14)	223	53 795.3998	136 776	0.002 602	CCD	(18)
160	51 615.0341	111 054	−0.001 976	CCD	(14)	224	53 827.6570	139 707	0.003 393	CCD	(21)
161	51 615.1260	111 055	0.003 907	CCD	(14)	225	54 079.7666	139 708	−0.003 098	CCD	(21)
162	51 615.2098	111 056	0.001 690	CCD	(14)	226	54 079.8580	139 709	0.002 285	CCD	(21)
163	51 615.2919	111 064	−0.002 227	CCD	(14)	227	54 079.9437	139 973	0.001 967	CCD	(21)
164	51 615.9855	111 065	0.003 236	CCD	(14)	228	54 102.6471	139 974	−0.003 144	CCD	(21)
165	51 616.0705	111 066	0.002 219	CCD	(14)	229	54 102.7365	139 975	0.000 238	CCD	(21)
166	51 616.1526	111 067	−0.001 698	CCD	(14)	230	54 102.8254	139 985	0.003 121	CCD	(21)
167	51 616.2389	114 706	−0.001 415	CCD	(14)	231	54 103.6849	139 986	0.002 450	CCD	(21)
168	51 929.2556	114 707	−0.000 886	CCD	(14)	232	54 103.7677	139 997	−0.000 767	CCD	(21)
169	51 929.3464	114 717	0.003 897	CCD	(14)	233	54 104.7117	140 031	−0.002 955	CCD	(21)
170	51 930.2058	114 718	0.003 126	CCD	(14)	234	54 107.6358	140 032	−0.003 436	CCD	(21)
171	51 930.2885	114 719	−0.000 191	CCD	(14)	235	54 107.7251	140 033	−0.000 153	CCD	(21)
172	51 930.3721	114 729	−0.002 608	CCD	(14)	236	54 107.8138	140 034	0.002 530	CCD	(21)
173	51 931.2315	114 730	−0.003 379	CCD	(14)	237	54 107.8944	140 067	−0.002 887	CCD	(21)
174	51 931.3203	114 845	−0.000 596	CCD	(14)	238	54 110.7388	140 068	0.002 949	CCD	(21)
175	51 941.2102	114 846	−0.002 661	CCD	(14)	239	54 110.8207	140 069	−0.001 168	CCD	(21)
176	51 941.2979	114 847	−0.000 978	CCD	(14)	240	54 110.9051	140 070	−0.002 785	CCD	(21)
177	51 941.3881	114 856	0.003 205	CCD	(14)	241	54 110.9977	140 241	0.003 798	CCD	(21)
178	51 942.1562	114 857	−0.002 849	CCD	(14)	242	54 125.7056	140 242	0.002 775	CCD	(21)

Table 7 – *continued*

NO.	$T_{\max}$	E	O − C	Det	S	NO.	$T_{\max}$	E	O − C	Det	S
243	54 125.7883	140 243	−0.000 542	CCD	(21)	307	54 770.8336	147 741	0.002 589	CCD	(21)
244	54 125.8716	140 244	−0.003 259	CCD	(21)	308	54 770.9152	147 742	−0.001 828	CCD	(21)
245	54 125.9649	140 309	0.004 024	CCD	(21)	309	54 781.8384	147 869	−0.002 798	CCD	(21)
246	54 131.5550	140 310	0.003 013	CCD	(21)	310	54 781.9301	147 870	0.002 884	CCD	(21)
247	54 131.6392	140 311	0.001 196	CCD	(21)	311	54 788.8080	147 950	−0.000 583	CCD	(21)
248	54 131.7212	140 312	−0.002 821	CCD	(21)	312	54 788.8912	147 951	−0.003 400	CCD	(21)
249	54 131.8106	140 313	0.000 562	CCD	(21)	313	54 788.9833	147 952	0.002 683	CCD	(21)
250	54 131.8989	140 367	0.002 845	CCD	(21)	314	54 791.7333	147 984	0.000 136	CCD	(21)
251	54 136.5446	140 368	0.003 622	CCD	(21)	315	54 791.8157	147 985	−0.003 481	CCD	(21)
252	54 136.6275	140 369	0.000 505	CCD	(21)	316	54 791.9080	147 986	0.002 802	CCD	(21)
253	54 136.7104	140 370	−0.002 612	CCD	(21)	317	54 791.9938	147 987	0.002 585	CCD	(21)
254	54 136.7998	140 371	0.000 771	CCD	(21)	318	54 807.8222	148 171	0.003 840	CCD	(21)
255	54 136.8882	140 372	0.003 154	CCD	(21)	319	54807.9032	148 172	−0.001 177	CCD	(21)
256	54 136.9697	140 380	−0.001 364	CCD	(21)	320	54 807.9866	148 173	−0.003 795	CCD	(21)
257	54 137.6581	140 381	−0.001 100	CCD	(21)	321	54 816.6793	148 274	0.001 179	CCD	(21)
258	54 137.7491	140 382	0.003 883	CCD	(21)	322	54 816.7612	148 275	−0.002 938	CCD	(21)
259	54 137.8311	140 404	−0.000 134	CCD	(21)	323	54 816.8501	148 276	−0.000 055	CCD	(21)
260	54 139.7226	140 405	−0.001 010	CCD	(21)	324	54 816.9399	148 277	0.003 728	CCD	(21)
261	54 139.8124	140 406	0.002 772	CCD	(21)	325	54 837.6637	148 518	−0.002 591	CCD	(21)
262	54 139.8942	140 428	−0.001 445	CCD	(21)	326	54 837.7565	14 8519	0.004 191	CCD	(21)
263	54 141.7876	140 429	−0.000 421	CCD	(21)	327	54 843.6886	148 588	0.001 112	CCD	(21)
264	54 141.8768	140 430	0.002 762	CCD	(21)	328	54 843.7704	148 589	−0.003 105	CCD	(21)
265	54 141.9575	140 554	−0.002 555	CCD	(21)	329	54 843.8567	148 590	−0.002 822	CCD	(21)
266	54 152.6241	140 565	−0.002 074	CCD	(21)	330	54 843.9494	148 591	0.003 861	CCD	(21)
267	54 153.5746	140 578	0.002 238	CCD	(21)	331	54 846.6137	148 622	0.001 631	CCD	(21)
268	54 154.6883	140 579	−0.002 284	CCD	(21)	332	54 846.6960	148 623	−0.002 086	CCD	(21)
269	54 154.7800	140 580	0.003 399	CCD	(21)	333	54 847.7336	148 635	0.003 309	CCD	(21)
270	54 154.8618	140 773	−0.000 818	CCD	(22)	334	54 847.8164	148 636	0.000 092	CCD	(21)
271	54 171.4664	140 808	0.002 483	CCD	(22)	335	54 847.8988	148 637	−0.003 525	CCD	(21)
272	54 175.4206	140 819	−0.000 103	CCD	(22)	336	54 855.6469	148 727	0.003 036	CCD	(21)
273	54 196.4976	141 064	0.00 2710	CCD	(22)	337	54 855.7316	148 728	0.001 719	CCD	(21)
274	54 197.3590	141 074	0.003 939	CCD	(22)	338	54 855.8119	148 729	−0.003 998	CCD	(21)
275	54 197.4402	141 075	−0.000 878	CCD	(22)	339	54 855.9023	148 730	0.000 385	CCD	(21)
276	54 198.3850	141 086	−0.002 266	CCD	(22)	340	54 864.5873	148 831	−0.002 341	CCD	(21)
277	54 198.4741	141 087	0.000 817	CCD	(22)	341	54 864.6724	148 832	−0.003 258	CCD	(21)
278	54 202.4288	141 133	−0.00 1270	CCD	(22)	342	54 864.7649	148 833	0.003 224	CCD	(21)
279	54 414.8939	143 603	0.00 1615	CCD	(21)	343	54 864.8477	148 834	0.000 007	CCD	(21)
280	54 414.9804	143 604	0.002 098	CCD	(21)	344	54 864.9296	148 835	−0.004 110	CCD	(21)
281	54 417.7271	143 636	−0.003 749	CCD	(21)	345	54 868.6346	148 878	0.002 155	CCD	(21)
282	54 417.9058	143 638	0.002 917	CCD	(21)	346	54 868.7166	148 879	−0.001 862	CCD	(21)
283	54 417.9856	143 639	−0.003 300	CCD	(21)	347	54868.8033	148 880	−0.001 179	CCD	(21)
284	54 440.6958	143 903	−0.001 612	CCD	(21)	348	54 868.8941	148 881	0.003 604	CCD	(21)
285	54 442.7619	143 927	0.000 078	CCD	(21)	349	54 878.6935	148 995	−0.002 945	CCD	(21)
286	54 442.8516	143 928	0.003761	CCD	(21)	350	54 878.7811	148 996	−0.001 362	CCD	(21)
287	54 442.9342	143 929	0.000 344	CCD	(21)	351	54 878.8721	148 997	0.003 621	CCD	(21)
288	54 451.6243	144 030	0.002 717	CCD	(21)	352	54894.4412	149 178	0.003 628	CCD	(24)
289	54 460.6513	144 135	−0.002 077	CCD	(21)	353	54894.5227	149 179	−0.000 890	CCD	(24)
290	54 460.7433	144 136	0.003 906	CCD	(21)	354	54 894.6071	149 180	−0.002 507	CCD	(24)
291	54 460.8247	144 137	−0.000 712	CCD	(21)	355	54 897.0188	149 208	0.000 058	CCD	(26)
292	54 460.9089	144 138	−0.002 529	CCD	(21)	356	54 897.1069	149 209	0.004 345	CCD	(26)
293	54 467.7955	144 218	0.002 704	CCD	(21)	357	54 897.1883	149 210	−0.000 972	CCD	(26)
294	54 468.7392	144 229	0.000 216	CCD	(21)	358	54 898.0490	149 220	−0.003 829	CCD	(26)
295	54 468.8220	144 230	−0.003 001	CCD	(21)	359	54 898.1331	149 221	0.004 153	CCD	(26)
296	54 468.9120	144 231	0.000 982	CCD	(21)	360	54 898.3084	149 223	−0.001 064	CCD	(24)
297	54 469.6815	144 240	−0.003 672	CCD	(21)	361	54 898.9930	149 231	−0.003 252	CCD	(26)
298	54 469.7701	144 241	−0.001 089	CCD	(21)	362	54 899.0837	149 232	0.003 172	CCD	(26)
299	54 469.8603	144 242	0.003 094	CCD	(21)	363	54 899.1706	149 233	−0.000 545	CCD	(26)
300	54 469.9414	144 243	−0.001 823	CCD	(21)	364	54 900.0318	149 243	0.002 679	CCD	(26)
301	54 506.5887	144 669	0.002 196	CCD	(23)	365	54 900.1128	149 244	0.002 702	CCD	(26)
302	54 512.5199	144 738	−0.001 784	CCD	(23)	366	54 900.1978	149 245	−0.002 250	CCD	(26)
303	54 513.4650	144 749	−0.002 872	CCD	(23)	367	54 901.0575	149 255	0.004 333	CCD	(26)
304	54 513.5559	144 750	0.002 011	CCD	(23)	368	54904.4199	149 294	0.001 172	CCD	(24)
305	54 524.4815	144 877	0.003 441	CCD	(23)	369	54 904.5006	149 295	−0.003 733	CCD	(24)
306	54 769.8859	147 730	0.001 077	CCD	(21)	370	54 909.3147	149 351	0.000 862	CCD	(24)

Table 7 – *continued*

NO.	T_{max}	E	O − C	Det	S	NO.	T_{max}	E	O − C	Det	S
371	54 909.4087	149 352	−0.003 555	CCD	(24)	417	55 617.3281	157 582	0.002 874	CCD	(26)
372	54 909.4895	149 353	−0.002 426	CCD	(24)	418	55 620.0772	157 614	−0.000 573	CCD	(26)
373	54 910.4335	149 364	−0.003 443	CCD	(24)	419	55 620.1602	157 615	−0.003 590	CCD	(26)
374	54 912.3323	149 386	0.000 770	CCD	(24)	420	55 621.1103	157 626	0.000 322	CCD	(26)
375	54 912.4146	149 387	−0.003 835	CCD	(24)	421	55 621.1986	157 627	0.002 604	CCD	(26)
376	54 924.3742	149 526	0.003 777	CCD	(24)	422	55 937.3981	161 303	0.003 264	CCD	(26)
377	54 970.0431	150 057	0.000 360	CCD	(26)	423	55 961.3051	161 581	−0.002 489	CCD	(26)
378	54 972.1078	150 081	0.000 715	CCD	(26)	424	55 961.3907	161 582	−0.002 906	CCD	(26)
379	55 230.2455	153 082	0.002 798	CCD	(26)	425	55 964.3148	161 616	−0.003 387	CCD	(26)
380	55 230.3379	153 083	−0.001 819	CCD	(26)	426	55 964.4073	161 617	0.003 096	CCD	(26)
381	55230.4201	153 084	−0.001 290	CCD	(26)	427	55 966.2133	161 638	0.002 737	CCD	(26)
382	55 231.2818	153 094	−0.003 207	CCD	(26)	428	55 966.2942	161 639	−0.002 380	CCD	(26)
383	55 231.3635	153 095	−0.003 478	CCD	(26)	429	55 966.3797	161 640	−0.002 897	CCD	(26)
384	55 259.4108	153 421	0.001 205	CCD	(25)	430	55 967.3311	161 651	0.002 315	CCD	(26)
385	55 293.3826	153 816	0.002 087	CCD	(25)	431	55 967.4159	161 652	0.001 098	CCD	(26)
386	55 293.4752	153 817	0.003 117	CCD	(25)	432	55 968.2773	161 662	0.002 327	CCD	(26)
387	55302.3318	153 920	−0.001901	CCD	(25)	433	55 968.3582	161 663	−0.002 790	CCD	(26)
388	55303.3591	153 932	−0.002 918	CCD\	(25)	434	55 969.3038	161 674	−0.003 379	CCD	(26)
389	55304.3959	153 944	−0.003 389	CCD	(25)	435	55 969.3959	161 675	0.002 704	CCD	(26)
390	55304.4775	153 945	−0.003 497	CCD	(25)	436	55 997.0080	161 996	0.003 317	CCD	(26)
391	55305.3388	153 955	−0.003 207	CCD	(25)	437	55 997.0906	161 997	−0.000 100	CCD	(26)
392	55305.4238	153 956	−0.002 804	CCD	(25)	438	55 997.1730	161 998	−0.003 717	CCD	(26)
393	55 309.3848	154 002	0.003 579	CCD	(25)	439	55 997.2639	161 999	0.001 166	CCD	(26)
394	55 310.4124	154 014	−0.000 238	CCD	(25)	440	55 998.0337	162 008	−0.003 188	CCD	(26)
395	55 311.3662	154 025	0.001 291	CCD	(25)	441	55 998.1221	162 009	−0.000 805	CCD	(26)
396	55 311.4488	154 026	−0.003 026	CCD	(25)	442	55 998.2119	162 010	0.002 977	CCD	(26)
397	55 583.4313	157 188	−0.003 191	CCD	(26)	443	55 998.2927	162 011	−0.00 2240	CCD	(26)
398	55 584.3787	157 199	−0.001 979	CCD	(26)	444	55 998.9808	162 019	−0.002 276	CCD	(26)
399	55 585.4132	157 211	0.000 316	CCD	(26)	445	55 999.0727	162 020	0.003 606	CCD	(26)
400	55 587.3946	157 234	0.003 323	CCD	(26)	446	55 999.1547	162 021	−0.000 411	CCD	(26)
401	55 588.4201	157 246	−0.003 383	CCD	(26)	447	55 999.2375	162 022	−0.003 628	CCD	(26)
402	55 607.9528	157 473	0.003 437	CCD	(26)	448	56 000.0161	162 031	0.000 818	CCD	(26)
403	55 608.0348	157 474	−0.000 580	CCD	(26)	449	56 000.0978	162 032	−0.003 499	CCD	(26)
404	55 608.1180	157 475	−0.003 397	CCD	(26)	450	56 000.1874	162 033	0.000 084	CCD	(26)
405	55 608.2099	157 476	0.002 486	CCD	(26)	451	56 000.2762	162 034	0.002 867	CCD	(26)
406	55 608.2954	157 477	0.001 969	CCD	(26)	452	56001.0459	162 043	−0.001 587	CCD	(26)
407	55 608.3763	157 478	−0.003 148	CCD	(26)	453	56 001.1368	162 044	0.003 296	CCD	(26)
408	55 610.3591	157 501	0.001 258	CCD	(26)	454	56 001.2186	162 045	−0.000 921	CCD	(26)
409	55 611.3877	157 513	−0.002347	CCD	(26)	455	56 001.3023	162 046	−0.003 238	CCD	(26)
410	55 612.2469	157 523	−0.003 318	CCD	(26)	456	56 062.0312	162 752	−0.002 407	CCD	(26)
411	55 612.3392	157 524	0.002 965	CCD	(26)	457	56 063.0691	162 764	0.003 287	CCD	(26)
412	55 613.1980	157 534	0.001 594	CCD	(26)	458	56 064.0137	162 775	0.001 699	CCD	(26)
413	55616.9800	157 578	−0.001 158	CCD	(26)	459	56 064.0948	162 776	−0.003 218	CCD	(26)
414	55 617.0705	157 579	0.003 325	CCD	(26)	460	56 065.0419	162 787	−0.002 306	CCD	(26)
415	55 617.1520	157 580	−0.001 192	CCD	(26)	461	56 068.0580	162 822	0.003 196	CCD	(26)
416	55 617.2358	157 581	−0.003 409	CCD	(26)						

1.30–2.70 $M_\odot$ after the MS and the post-MS (before the red giant phase).

As a result, we got the models that included the frequencies f_0 and f_1 along with the stellar evolution tracks. These tracks provided the relevant intervals of the parameters for subsequent calculations, as listed in Table 10.

With the observations and the method used, one can believe that [Fe/H] and $\log g$ values have good reliability (Strömgren 1956; Crawford & Mander 1966). So, we decide to take the value [Fe/H] $= -0.3$ in our calculation.

We used the formula (with the solar metallicity $X_\odot = 0.7381$, $Y_\odot = 0.2485$ and $Z_\odot = 0.0134$ from Asplund et al. 2009)

$$[\mathrm{Fe/H}] = \log\left(\frac{Z}{X}\right) - \log\left(\frac{Z_\odot}{X_\odot}\right) \quad (6)$$

and the formula

$$X + Y + Z = 1 \quad (7)$$

to calculate the initial Z. In Girardi et al. (2000), a model was calculated with a couple of values $(Y, Z) = (0.25, 0.008)$, which are in accord with the values in our previous calculation (derived using MESA *astero* with the value of [Fe/H]).

At last, by integrating all the information about the value of (Y, Z), we decide to choose $(Y, Z) = (0.25, 0.008\,521)$ as the unique initial value for the subsequent calculation.

5.3 Constraints from the period variation

Unlike the solar-like stars for which many frequencies are detected, most HADS are observed with only the fundamental and

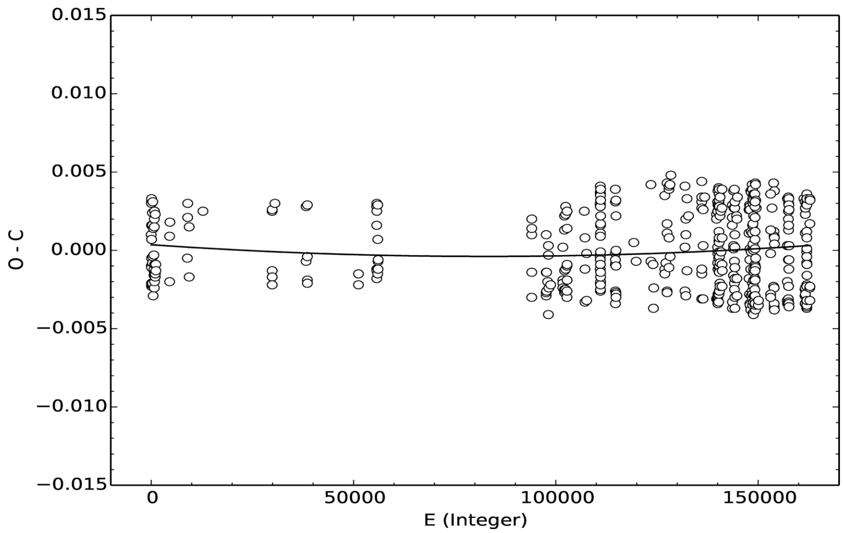

Figure 6. O − C diagram of AE UMa. The O − C values are in days. E is the cycle number. The solid curve shows the fit concerning a continuous increasing period change.

Table 8. Physical parameters of AE UMa from Rodriguez et al. (1992) and Hintz et al. (1997b). The $\log(L/\mathrm{L}_\odot)$ value was derived based on $\log(L/\mathrm{L}_\odot) = 0.4(M_{\mathrm{bol}_\odot} - M_{\mathrm{bol}})$.

Parameters	Mean value	Intervals	3σ
[Fe/H]	−0.3	[−0.4, −0.1]	–
T_{eff} (K)	7569	[7150, 8320]	[5980, 9490]
$\log g$	3.90	[3.77, 4.16]	[3.38, 4.55]
M_{bol}	–	[1.53, 1.93]	[1.33, 2.13]
$M(\mathrm{M}_\odot)$	–	[1.75, 1.95]	–
$\log(L/\mathrm{L}_\odot)$	–	[1.16, 1.32]	[1.08, 1.40]

Table 9. The parameters of the grid of model to search for f_0 and f_1. Since the values of M_{bol} and $\log(L/\mathrm{L}_\odot)$ in Table 6 were calculated from the stellar models of Rodriguez et al. (1992), and from observations, which depended on the models they used, we did not use these values as the constraints during our calculation.

Parameters	Maximum	Minimum	Step
[Fe/H]	−0.1	−0.4	0.05
Initial Y	0.33	0.23	0.02
Mass	2.7	1.3	0.02
$\log T_{\mathrm{eff}}$	3.977	3.777	–
$\log g$	4.55	3.38	–

Table 10. The parameters determined with the constraints from f_0 and f_1. The grid was constructed also within the parameter intervals of T_{eff} and $\log g$ listed in Table 6. In order to show an obvious comparison of the evolutionary tracks, we calculated the tracks with the stellar mass from 1.30 to 2.30 $\mathrm{M}_\odot$.

Parameters	Maximum	Minimum
[Fe/H]	− 0.2	− 0.4
Initial Y	0.27	0.23
Mass	2.26	1.32

Table 11. Physical parameters of AE UMa obtained from our calculation.

Parameter	Value	Uncertainty (per cent)
Mass ($\mathrm{M}_\odot$)	1.805 ± 0.055	3.04
Age (10^9 yr)	1.055 ± 0.095	9.00
$\log T_{\mathrm{eff}}$	3.922 ± 0.01	0.25
Radius (10^{11} cm)	1.647 ± 0.032	1.94
$\log g$	3.9543 ± 0.0044	0.11
$\log L$	1.381 ± 0.048	3.51

the first overtone modes in general (e.g. Balona et al. 2012; Ulusoy et al. 2013). As a result, the period variation becomes a very important constraint on the model calculation of these stars. High-precision detection of period variation may offer strong constraints on AE UMa. We used two independent ways to calculate the period variations of AE UMa theoretically.

5.3.1 *Calculation from stellar evolutionary effect*

The variation rate of the fundamental period derived from the long time-scale of observations of AE UMa shows a positive period change. From the theoretical point of view, the period changes caused by stellar evolution in and across the lower instability strip permit an observational test of stellar evolution theory (Breger & Pamyatnykh 1998).

The period–luminosity–colour relation can be expressed as (Breger & Pamyatnykh 1998)

$$\log P = -0.3M_{\mathrm{bol}} - 3\log T_{\mathrm{eff}} - 0.5\log M + \log Q + \mathrm{constant}, \quad (8)$$

where P is the period of a radial mode of pulsation, M_{bol} is the bolometric absolute magnitude, T_{eff} is the effective temperature, M is the stellar mass in solar mass and Q is the pulsation constant in days. For δ Scuti stars with radial pulsation, the constant is 12.708. For individual stars, the evolutionary period changes over long

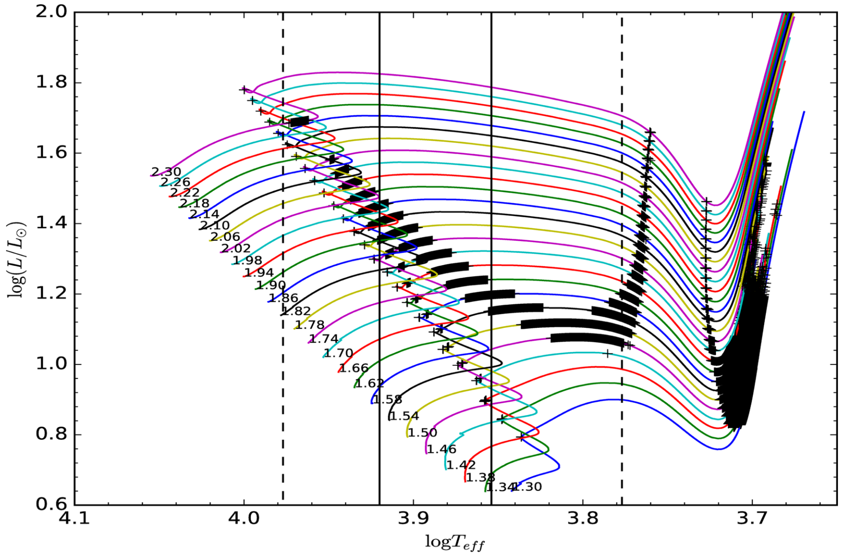

Figure 7. Evolutionary tracks of models with mass from 1.30 to 2.30 $M_\odot$ for (Y, Z) = (0.25, 0.008521). The solid and dashed vertical lines on the Hertzsprung–Russell diagram are determined from the observed $T_{\rm eff}$ in 1σ and 3σ, respectively. The marks on the tracks indicate the models with the values of the evolutionary period changes of $(1/P_0)(\mathrm{d}P_0/\mathrm{d}t)$ inside the interval (3.5210×10^{-9}, 7.2448×10^{-9}) in units of yr^{-1}. Note that the tracks are shown in the diagram with the mass interval of 0.04 $M_\odot$.

time-scales. An evolutionary change in $T_{\rm eff}$, $M_{\rm bol}$ and M leads to a period change of

$$\frac{1}{P}\frac{\mathrm{d}P}{\mathrm{d}t} = -0.69\frac{\mathrm{d}M_{\rm bol}}{\mathrm{d}t} - \frac{3}{T_{\rm eff}} - 0.5\frac{1}{M}\frac{\mathrm{d}M}{\mathrm{d}t} + \frac{1}{Q}\frac{\mathrm{d}Q}{\mathrm{d}t}. \tag{9}$$

Assuming that the stellar mass M = constant for δ Scuti stars during the observation interval with mass in the range of 1.30–2.30 $M_\odot$ and that the variation of pulsation constant is negligible, Yang et al. (2012) got

$$\frac{1}{P}\frac{\mathrm{d}P}{\mathrm{d}t} \approx -0.69\frac{\mathrm{d}M_{\rm bol}}{\mathrm{d}t} - \frac{3}{T_{\rm eff}}\frac{\mathrm{d}T_{\rm eff}}{\mathrm{d}t}. \tag{10}$$

As indicated by Rodríguez & Breger (2001), the HADS locate on or near the MS of the Hertzsprung–Russell diagram. Consequently, the evolutionary models are constructed from the pre-MS Hayashi phase to the end of the MS. The effect of rotation was not considered here for mainly two reasons: (1) The HADS typically have slow rotation, and most have a projected rotational velocity, $V\sin i$, of around 20 km s^{-1} (see, e.g. Solano & Fernley 1997). (2) The effects of rotation with a speed of $V\sin i$ = 18 km s^{-1} in HADS are very similar to those in the absence of rotation (Casas et al. 2006).

The evolutionary tracks constructed from 1.30 to 2.30 $M_\odot$ are shown in Fig. 7, and the corresponding variation rates of the period are marked.

As shown in Fig. 7, the states whose values of period changes are consistent with the observed ones determined from the O − C analysis lie just after the second turn-offs leaving the MSs on the evolutionary tracks.

5.3.2 *Calculation from* ADIPLS

ADIPLS (the Aarhus adiabatic oscillation package) is a program for the calculation of adiabatic oscillations of stellar models (Christensen-Dalsgaard 2008). We used it to calculate the frequencies of the eigenmodes of the model at each step of our evolutionary state. As a result, we got the frequencies of the model of F_0 and F_1 and then deduced the variation of those frequencies. In the calculation, the input frequencies F_0 and F_1 are the fundamental and first overtone frequencies with quantum numbers of l = 0 and n = 1, 2, respectively.

We calculated the evolutionary tracks from 1.30 to 2.30 $M_\odot$, and got the frequency values on each tracks, as shown in Fig. 8. Figs 8(a) and (b) show that the models with appropriate frequencies for AE UMa could appear (i) just before the first turn-offs, (ii) after the first and before the second turn-offs and (iii) just after the second turn-offs. We integrated the constraints from f_0 and f_1 and got the results shown in Fig. 8(c).

In addition, we also calculated the variations of the frequencies of the eigenmodes of the models by using ADIPLS. Adding the constraints from $(1/P_0)(\mathrm{d}P_0/\mathrm{d}t)$, which are thought to be due to the evolutionary effects, we got the results in Fig. 9.

One can find that this result is almost consistent with the result from Fig. 7 just after the second turn-off. The differences arise from the fact that we did not consider the variation of the stellar mass and the pulsation constant along the evolutionary tracks in Fig. 7.

Finally, we combined the constraints from f_0, f_1 and $(1/P_0)(\mathrm{d}P_0/\mathrm{d}t)$, and got the results shown in Fig. 10. One concludes that AE UMa should locate after the second turn-offs of the evolutionary tracks leaving the MS. Hence, one finds that the period variations of the fundamental mode of AE UMa are caused by the evolutionary effect. The rate of variation is consistent with the theoretically predicted value by Breger & Pamyatnykh (1998).

With the discussion above and constraints from the physical parameters, one can conclude that the mass of AE UMa ranges from 1.75 to 1.86 $M_\odot$ and the age from 0.96×10^9 to 1.15×10^9 yr.

We chose 1.80 $M_\odot$ as a sample to study the evolutionary state and the interior of the models that we gained. More details of the parameters we got from calculations are listed in Table 11. Fig. 11 shows the distribution of H, He^3 and He^4 versus the stellar radius.

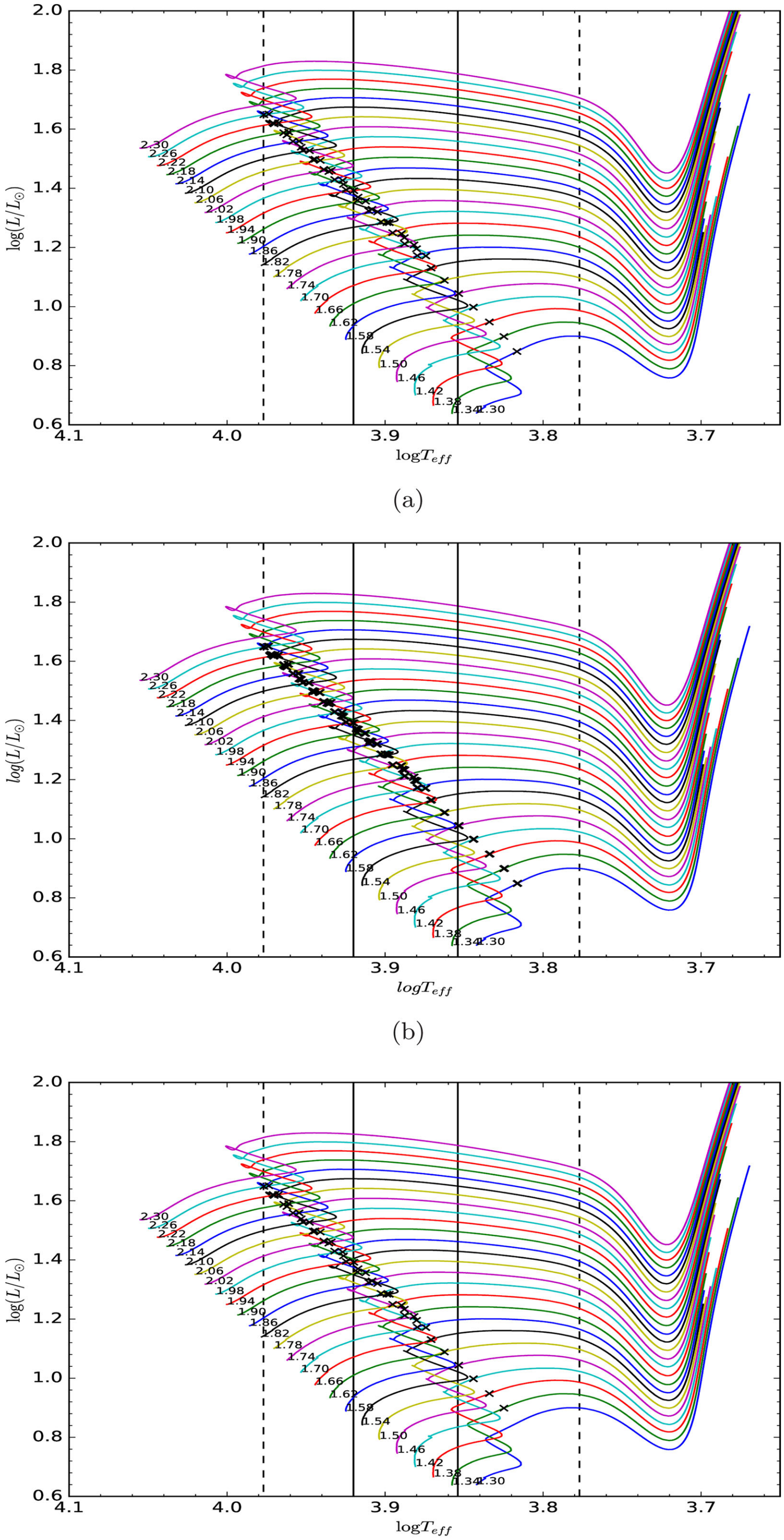

(a)

(b)

(c)

Figure 8. Models with the values of F_0 and F_1 calculated from ADIPLS, consistent with the observed ones ($F_0 \in [f_0 - 3\sigma, f_0 + 3\sigma]$ and $F_1 \in [f_1 - 3\sigma, f_1 + 3\sigma]$) are marked on the evolutionary tracks. (a) For $F_0 \in [f_0 - 3\sigma, f_0 + 3\sigma]$; (b) for $F_1 \in [f_1 - 3\sigma, f_1 + 3\sigma]$; and (c) for both $F_0 \in [f_0 - 3\sigma, f_0 + 3\sigma]$ and $F_1 \in [f_1 - 3\sigma, f_1 + 3\sigma]$.

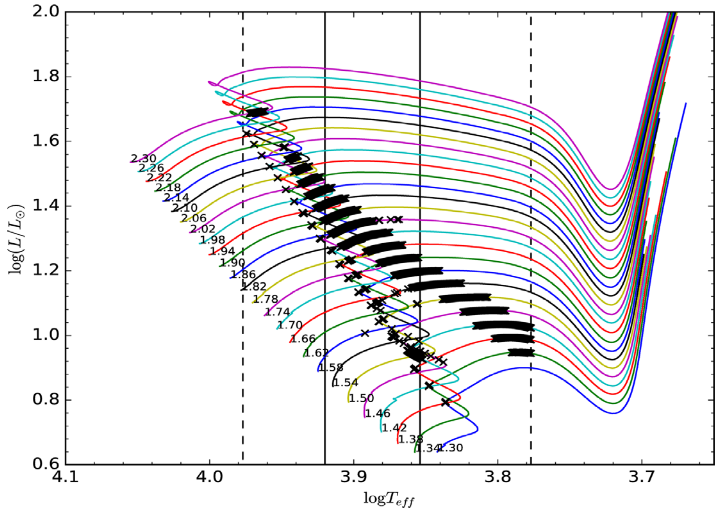

Figure 9. The models for which the period variations of the fundamental mode $(1/P_0)(dP_0/dt)$ calculated with ADIPLS agree with the observed values of $5.3829(\pm1.8619) \times 10^{-9}$ yr^{-1} are marked on the evolutionary tracks.

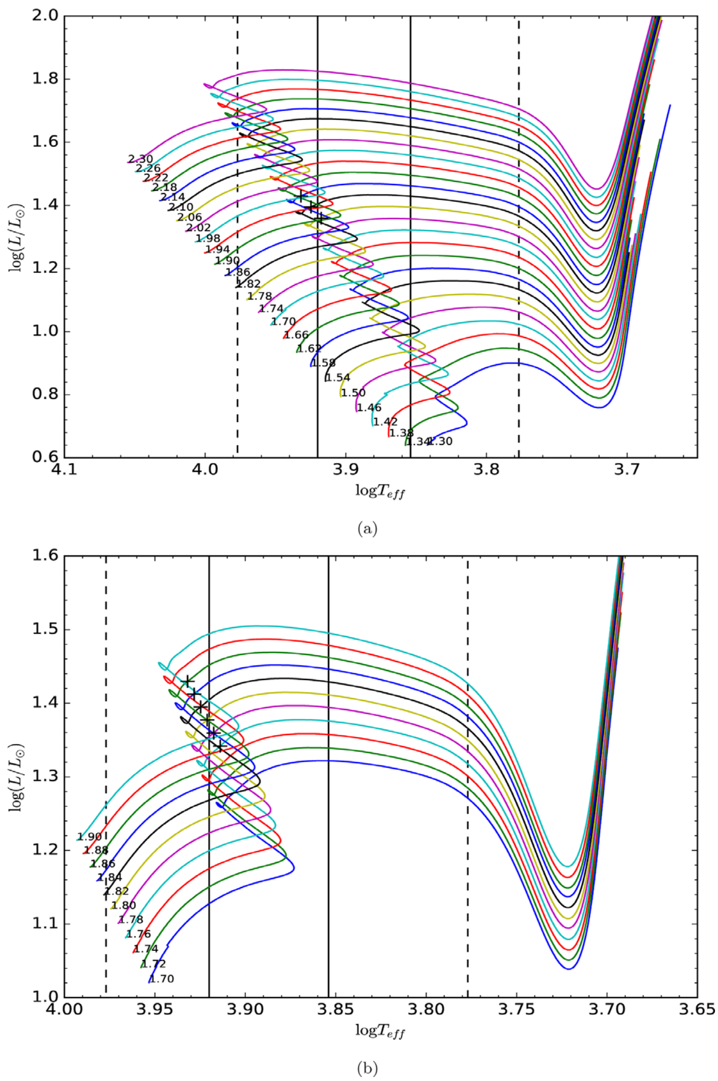

Figure 10. Evolutionary tracks of star models. (a) Marks on the tracks indicate the models with constraints from f_0, f_1 and $(1/P_0)(dP_0/dt)$. (b) A zoom-in of (a).

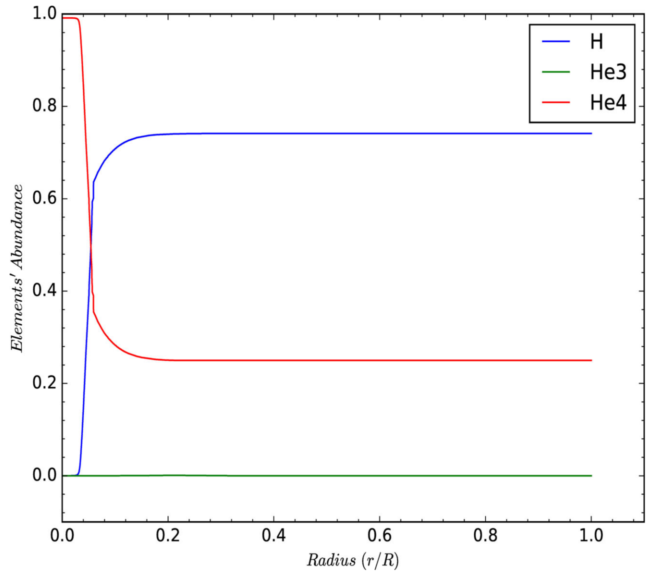

Figure 11. Elements' abundance distribution of H, He^3 and He^4 inside the star for the model with the star mass of 1.80 $M_\odot$.

Fig. 12 presents the energy distribution inside the star. From Figs 11 and 12, one may find that the star should have a helium core and a hydrogen-burning shell.

We also calculated models with different values of Y, Z and α_{ov} by using different grids. The result showed that the states were not different significantly. All the results pointed out that AE UMa should lie just after the second turn-off with a helium core and a hydrogen-burning shell.

6 CONCLUSIONS

We analyse the photometric data gathered on AE UMa over 40 nights spanning from 2009 to 2012 and detect 37 frequencies above the so-called 4σ detection threshold, among which 25 frequencies are newly detected. All these frequencies are linked to either harmonics or linear combinations of the two main frequencies $f_0 = 11.625\,60$ c d^{-1} and $f_1 = 15.031\,23$ c d^{-1}, corresponding to the fundamental and the first overtone radial pulsation modes, respectively. No frequencies of the other pulsation modes were detected from the observed data.

An O − C diagram is constructed from a combination of the 84 times of maximum light determined from our new observations and 360 times listed in the literature, leading to the updated value of period $P_0 = 0.086\,017\,0781$ d. A new ephemeris with a quadratic solution suggests that the period change rate of the fundamental mode of AE UMa is of $(1/P_0)(\mathrm{d}P_0/\mathrm{d}t) = 5.4(\pm1.9) \times 10^{-9}$ yr^{-1}. The value is different from the result obtained by Zhou (2001) and needs to be confirmed with more data that will be collected from observations in the near future, both from ground and space (e.g. *TESS*; Ricker et al. 2014). Because the large values of the derivative of $(1/P_1)(\mathrm{d}P_1/\mathrm{d}t)$ were obtained from the standard O − C method, we did not use this value as a constraint in the model calculation.

With the spectroscopic observation data, we got the low-resolution spectrum and used the automated 1D parametrization pipeline LASP to obtain the stellar atmospheric parameters of AE UMa. These parameters (especially the [Fe/H] value of −0.32) certify that AE UMa is a Population I δ Scuti star rather than a Population II SX Phe star.

We then calculated models of stars with masses between 1.30 and 2.70 $M_\odot$. With the constraints of the values of f_0, f_1 and $(1/P_0)(\mathrm{d}P_0/\mathrm{d}t)$, we conclude that AE UMa lies just after the second turn-offs of the evolutionary tracks leaving the MS. The

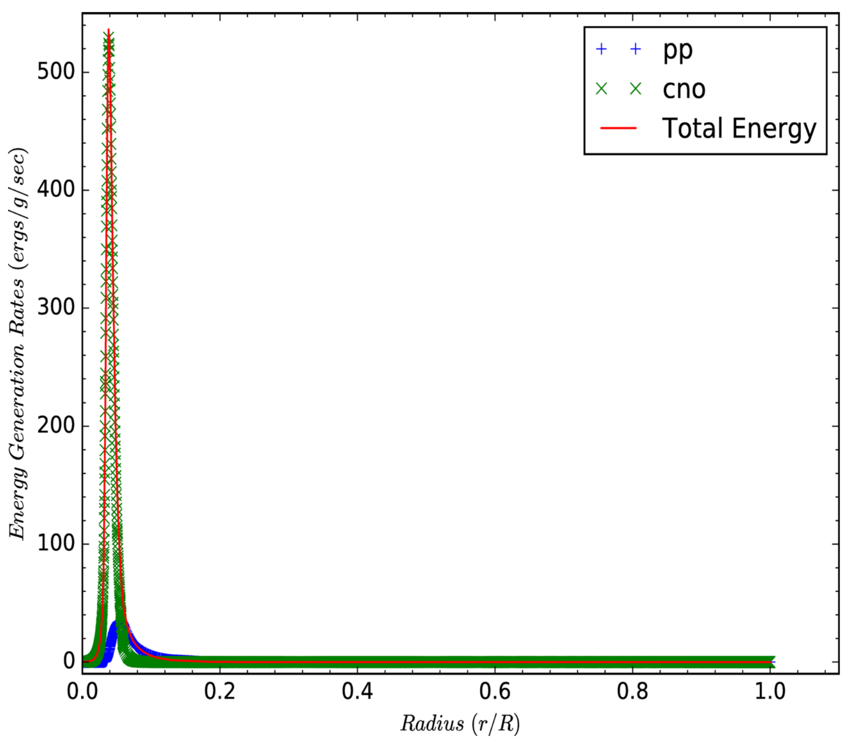

Figure 12. Energy generation rate distribution inside the star for the model with the star mass of 1.80 $M_\odot$.

corresponding mass should be $1.805 \pm 0.055\,M_{\odot}$ and the age $1.055 \pm 0.095 \times 10^{9}$ yr. At this evolutionary phase, the star should have a helium core and a hydrogen-burning shell.

Moreover, according to the concrete observational evidence, we provide an example of the HADS whose evolutionary stage is on the post-MS. This gives a direct support to the general consensus that δ Scuti stars are probably normal stars evolving in the MS or the immediate post-MS stages.

ACKNOWLEDGEMENTS

J-SN and J-NF acknowledge the support from the Joint Fund of Astronomy of National Natural Science Foundation of China (NSFC) and Chinese Academy of Sciences through the grant U1231202, the NSFC grant 11673003, the National Basic Research Program of China (973 Program 2014CB845700 and 2013CB834900) and the LAMOST FELLOWSHIP supported by the Special Funding for Advanced Users, budgeted and administrated by the Center for Astronomical Mega-Science, Chinese Academy of Sciences (CAMS). J-SN thanks Nami Mowlavi for helpful discussions and useful advice.

REFERENCES

Agerer F., Hubscher J., 2003, Inf. Bull. Var. Stars, 5485, 1
Agerer F., Dahm M., Hubscher J., 1999a, Inf. Bull. Var. Stars, 4712, 1
Agerer F., Dahm M., Hubscher J., 1999b, Inf. Bull. Var. Stars, 4712, 1
Asplund M., Grevesse N., Sauval A. J., Scott P., 2009, ARA&A, 47, 481
Baglin A., Breger M., Chevalier C., Hauck B., Le Contel J. M., Sareyan J. P., Valtier J. C., 1973, A&A, 23, 221
Bahcall J. N., 1997, Phys. Rev. C, 56, 3391
Bahcall J. N., 2002, Phys. Rev. C, 65, 025801
Balona L. A. et al., 2012, MNRAS, 419, 3028
Braune W., Mundry E., 1982, BAV Mitt. Nr., 34
Braune W., Huebscher J., Mundry E., 1979, Astron. Nachr., 300, 165
Breger M., 1979, PASP, 91, 5
Breger M., 1980, ApJ, 235, 153
Breger M., 2000, in Breger M., Montgomery M., eds, ASP Conf. Ser. Vol. 210, Delta Scuti and Related Stars. Astron. Soc. Pac., San Francisco, p. 3
Breger M., Pamyatnykh A. A., 1998, A&A, 332, 958
Breger M. et al., 1993, A&A, 271, 482
Broglia P., Conconi P., 1975, A&AS, 22, 243
Casas R., Suárez J. C., Moya A., Garrido R., 2006, A&A, 455, 1019
Christensen-Dalsgaard J., 2008, Ap&SS, 316, 113
Claret A., Rodriguez E., Rolland A., Lopez de Coca P., 1990, in Cacciari C., Clementini G., eds, ASP Conf. Ser. Vol. 11, Confrontation Between Stellar Pulsation and Evolution. Astron. Soc. Pac., San Francisco, p. 481
Crawford D. L., Mander J., 1966, AJ, 71, 114
Ferguson J. W., Alexander D. R., Allard F., Barman T., Bodnarik J. G., Hauschildt P. H., Heffner-Wong A., Tamanai A., 2005, ApJ, 623, 585
Filatov G. S., 1960, Astron. Nachr., 215, 20
Fu J. N. et al., 2008b, AJ, 135, 1958
Fu J.-N., Zhang C., Marak K., Boonyarak C., Khokhuntod P., Jiang S.-Y., 2008a, Chinese J. Astron. Astrophys., 8, 237
Garcia J. R. et al., 1995, A&AS, 109, 201
Geyer E., Kippenhahn R., Strohmeier W., 1955, Kleine Veröff, Bamberg, No. 11
Girardi L., Bressan A., Bertelli G., Chiosi C., 2000, A&AS, 141, 371
Götz W., Wenzel W., 1961, Mitt. Veränd. Sterne, No. 571
Herwig F., 2000, A&A, 360, 952
Hintz E. G., Joner M. D., McNamara D. H., Nelson K. A., Moody J. W., Kim C., 1997a, PASP, 109, 15
Hintz E., Hintz M. L., Joner M. D., 1997b, PASP, 109, 1073
Hubscher J., 2005, Inf. Bull. Var. Stars, 5643, 1
Hubscher J., 2007, Inf. Bull. Var. Stars, 5802, 1
Hubscher J., Walter F., 2007, Inf. Bull. Var. Stars, 5761, 1
Hübscher J., Agerer F., Wunder E., 1992, BAV Mitt., Nr., 60
Hubscher J., Paschke A., Walter F., 2005, Inf. Bull. Var. Stars, 5657, 1
Hubscher J., Paschke A., Walter F., 2006, Inf. Bull. Var. Stars, 5731, 1
Hubscher J., Steinbach H.-M., Walter F., 2009, Inf. Bull. Var. Stars, 5874, 1
Hubscher J., Lehmann P. B., Monninger G., Steinbach H.-M., Walter F., 2010, Inf. Bull. Var. Stars, 5918, 1
Huebscher J., Monninger G., 2011, BAV Mitt., 214, 1
Huebscher J., Lichtenknecker D., Mundry E., 1985, BAV Mitt., Nr., 39
Iglesias C. A., Rogers F. J., 1993, ApJ, 412, 752
Iglesias C. A., Rogers F. J., 1996, ApJ, 464, 943
Kepler S. O., Castanheira B. G., Saraiva M. F. O., Nitta A., Kleinman S. J., Mullally F., Winget D. E., Eisenstein D. J., 2005, A&A, 442, 629
Klingenberg G., Dvorak S. W., Robertson C. W., 2006, Inf. Bull. Var. Stars, 5701, 1
Lenz P., Breger M., 2005, Commun. Asteroseismol., 146, 53
Niu J.-S., Fu J.-N., Zong W.-K., 2013, Res. Astron. Astrophys., 13, 1181
Paxton B., Bildsten L., Dotter A., Herwig F., Lesaffre P., Timmes F., 2011, ApJS, 192, 3
Paxton B. et al., 2013, A&AS, 208, 4
Pejcha O., Havlik T., Kral L., 2001, Inf. Bull. Var. Stars, 5080, 1
Petersen J. O., Christensen-Dalsgaard J., 1996, A&A, 312, 463
Pócs M. D., Szeidl B., 2001, A&A, 368, 880
Poretti E., 2003, A&A, 409, 1031
Pringle J. E., 1975, MNRAS, 170, 633
Ricker G. R. et al., 2014, in Oschmann J. M. Jr., Clampin M., Fazio G. G., MacEwen H. A., Proc. SPIE Conf. Ser. Vol. 9143, Space Telescopes and Instrumentation 2014: Optical, Infrared, and Millimeter Wave. SPIE, Bellingham, p. 914320
Rodríguez E., Breger M., 2001, A&A, 366, 178
Rodríguez E., López-González M. J., 2000, A&A, 359, 597
Rodriguez E., Rolland A., Lopez de Coca P., Garcia-Lobo E., Sedano J. L., 1992, A&AS, 93, 189
Rogers F. J., Nayfonov A., 2002, ApJ, 576, 1064
Samolyk G., 2010, J. Am. Assoc. Var. Star Obs., 38, 12
Saumon D., Chabrier G., van Horn H. M., 1995, ApJS, 99, 713
Seaton M. J., 2005, MNRAS, 362, L1
Solano E., Fernley J., 1997, A&AS, 122
Strömgren B., 1956, Vistas Astron., 2, 1336
Szeidl B., 1974, Inf. Bull. Var. Stars, 903, 1
Tsesevich V. P., 1973, Astronomicheskij Tsirkulyar, 775, 2
Ulusoy C. et al., 2013, MNRAS, 433, 394
Wenger M. et al., 2000, A&AS, 143, 9
Wu Y. et al., 2011, Res. Astron. Astrophys., 11, 924
Yang X. H., Fu J. N., Zha Q., 2012, AJ, 144, 92
Zhou A.-Y., 2001, A&A, 374, 235
Zhou A.-Y., Jiang X.-J., Zhang Y.-P., Wei J.-Y., 2009, Res. Astron. Astrophys., 9, 349
Zong W. et al., 2015, AJ, 149, 84

This paper has been typeset from a TEX/LATEX file prepared by the author.